Inorg. Chem. **2006**, *45*, 4284–4302

Assembly of Heterometallic Clusters and Coordination Polymers by Combining Mo–S-Based Clusters with Mn^{2+}

Ping Lin, William Clegg, Ross W. Harrington, Richard A. Henderson,* Ashleigh J. Fletcher, Jon Bell, and K. Mark Thomas

Chemisty, School of Natural Sciences, University of Newcastle, Newcastle upon Tyne, NE1 7RU, U.K.

Received February 6, 2006

Addition of $[Mo^{V}_2O_2S_2(edt)_2]^{2-}$ (edt = 1,2-ethanedithiolate) to acetonitrile and/or methanol solutions of Mn^{II} containing bipyridines [4,4′-trimethylenedipyridine (TDP), 4,4′-bipyridine (4,4′-bpy), 2,2′-bipyridine (2,2′-bpy)] or 15-crown-5 produces three new heterometallic cluster coordination polymers, $[Mn_2\{Mo_2O_2S_2(edt)_2\}_2(TDP)_3(CH_3OH)_2(NCMe)_2]\cdot 3CH_3OH\cdot 0.25MeCN$ (**1**), $[Mn(TDP)_2(H_2O)_2]^{2+}[Mn\{Mo_2O_2S_2(edt)_2\}_2(TDP)_2\}]^{2-}\cdot 6CH_3OH$ (**2**), $[Mn\{Mo_2O_2S_2(edt)_2\}(TDP)_2(CH_3OH)(H_2O)]\cdot CH_3OH$ (**3**), and three new multinuclear clusters, $[Mn\{Mo_2O_2S_2(edt)_2\}(4,4'\text{-bpy})(CH_3OH)_4]\cdot 0.5(4,4'\text{-bpy})$ (**4**), $[Mn\{Mo_2O_2S_2(edt)_2\}(2,2'\text{-bpy})_2]\cdot 2CH_3OH$ (**5**), and $(NEt_4)_2[Mn(15\text{-crown-}5)\{Mo_2O_2S_2(edt)_2\}_2]$ (**6**). All compounds were characterized by X-ray crystallography. The coordination mode of Mn in these compounds depends on the ligands and the crystallization conditions. Compound **2** readily converts to **1** or **3** depending on the reaction and solvent conditions. Compounds **1** and **2** were analyzed using thermogravimetric analysis combined with mass spectroscopy (TG-MS) in the temperature range 25–500 °C. The room-temperature magnetic moments for compounds **1**–**6** were determined.

Introduction

Organic−inorganic hybrid materials can produce a variety of novel structures[1] and have potential applications in host−guest chemistry,[2] catalysis,[3] electrical conductivity,[4] and adsorption.[5] Most of the organic−inorganic hybrid materials reported so far are constructed from mononuclear metal centers with multiconnected ligands. Less attention has been paid to the use of metal clusters as building units for the synthesis of new multidimensional structures. Coordination polymers constructed with metal clusters as building blocks are usually relatively stable and, hence, more promising candidates for applications than those assembled with mononuclear metal centers.[6]

For the past 20 years the thiometalates of molybdenum(VI) and tungsten(VI), $[MXS_3]^{n-}$ (X = O, S, n = 2; X = $HB(C_3H_3N_2)_3$ or C_5Me_5, n = 1), have been extensively used

* To whom correspondence should be addressed. E-mail: r.a.henderson@ncl.ac.uk.

(1) (a) Batten, S. R.; Robson, R. *Angew. Chem., Int. Ed.* **1998**, *37*, 1460. (b) Blake, A. J.; Champness, N. R.; Hubberstey, P.; Li, W.-S.; Withersby, M. A.; Schröder, M. *Coord. Chem. Rev.* **1999**, *183*, 117. (c) Carlucci, L.; Ciani, G.; Moret, M.; Proserpio, D. M.; Rizzato, S. *Angew. Chem., Int. Ed.* **2000**, *39*, 1506. (d) Zaworotko, M. J. *Chem. Commun.* **2001**, 1. (e) Zaworotko, M. J. *Chem. Soc. Rev.* **1994**, 283. (f) Hagrman, P. J.; Hagrman, D.; Zubieta, J. *Angew. Chem., Int. Ed.* **1999**, *38*, 2638. (g) Carlucci, L.; Ciani, G.; Gudenberg, D. W. V.; Proserpio, D. M. *Inorg. Chem.* **1997**, *36*, 3812.

(2) (a) Yaghi, O. M.; Li, G.-M.; Li, H.-L. *Nature*, **1995**, *378*, 703. (b) Fujita, M. *Chem. Soc. Rev.* **1998**, *27*, 417. (c) Kepert, C. J.; Prior, T. J.; Rosseinsky, M. J. *J. Am. Chem. Soc.* **2000**, *122*, 5158. (d) Kiang, Y.-H.; Gardner, G. B.; Lee, S.; Xu, Z.-T.; Lobkovsky, E. B. *J. Am. Chem. Soc.* **1999**, *121*, 8204. (e) Duncan, P. C. M.; Goodgame, D. M. L.; Menzer, S.; Willams, D. J. *Chem. Commun.* **1996**, 2127.

(3) (a) Fujita, M.; Kwon, Y. J.; Washizu, S.; Ogura, K. *J. Am. Chem. Soc.* **1994**, *116*, 1151. (b) Kesanli, B.; Lin, W.-B. C*oord. Chem. Rev.* **2003**, *246*, 305.

(4) (a) Su, W.-P., Hong, M.-C.; Weng, J.-B.; Cao, R.; Lu, S.-F. *Angew. Chem., Int. Ed.* **2000**, *39*, 2911. (b) Lin, P.; Henderson, R. A.; Harrington, R. W.; Clegg, W.; Wu, C.-D.; Wu, X.-T. *Inorg. Chem.* **2004**, *43*, 181. (c) Liu, S.-Q.; Kuroda-Sowa, T.; Konaka, H.; Suenaga, Y.; Maekawa, M.; Mizutani, T.; Ning, G.-L.; Munakata, M. *Inorg. Chem.* **2005**, *44*, 1031.

(5) (a) Zhao, X.-B.; Xiao, B.; Fletcher, A. J.; Thomas, K. M.; Bradshaw, D.; Rosseinsky, M. J. *Science* **2004**, *306*, 1012. (b) Dybtsev, D. N.; Chun, H.; Yoon, S.-H.; Kim, D.; Kim, K. *J. Am. Chem. Soc.* **2004**, *126*, 32. (c) Pan, L.; Sander, M. B.; Huang, X.-Y.; Li, J.; Milton, S.; Bittner, E.; Bockrath, B.; Johnson, J. K. *J. Am. Chem. Soc.* **2004**, *126*, 1308. (d) Kondo, M.; Yoshitomi, T.; Seki, K.; Matsuzaka, H.; Kitagawa, S. *Angew. Chem., Int. Ed. Engl.* **1997**, *36*, 1725. (e) Fletcher, A. J.; Cussen, E. J.; Bradshaw, D.; Rosseinsky, M. J.; Thomas, K. M. *J. Am. Chem. Soc.* **2004**, *126*, 9750. (f) Halder, G. J.; Kepert, C. J. *J. Am. Chem. Soc.* **2005**, *127*, 7891. (g) Noro, S.; Kitagawa, S.; Kondo, M.; Seki, K. *Angew. Chem., Int. Ed.* **2000**, *39*, 2081.

(6) (a) Li, H.; Eddaoudi, M.; O'Keeffe, M.; Yaghi, O. M. *Nature* **1999**, *402*, 276. (b) Eddaoudi, M.; Kim, J.; Rosi, N.; Vodak, D.; Wachter, J.; O'Keeffe, M.; Yaghi, O. M. *Science* **2002**, *295*, 469. (c) Rowsell, J. L. C.; Millward, A. R.; Park, K. S.; Yaghi, O. M. *J. Am. Chem. Soc.* **2004**, *126*, 5666. (d) Rowsell, J. L. C.; Yaghi, O. M. *Angew. Chem., Int. Ed.* **2005**, *44*, 4670. (e) Miyasaka, H.; Nakata, K.; Sugiura, K.; Yamashita, M.; Clérac, R. *Angew. Chem., Int. Ed.* **2004**, *43*, 707. (f) Zheng, N.-F.; Bu, X.-H.; Feng, P.-Y. *J. Am. Chem. Soc.* **2002**, *124*, 9688.

10.1021/ic060205u CCC: $33.50 © 2006 American Chemical Society
Published on Web 04/13/2006

to prepare a range of structurally diverse heterometallic sulfido clusters and coordination polymers.[7−9] Many of these compounds are of interest because of their relevance to biological systems (active sites in metalloenzymes) and industrial applications (hydrodesulfurization in petrochemistry)[9−11] or potential applications in conductive[12] and nonlinear optical materials.[13] A general feature of the reactions of $[MoOS_3]^{2-}$ and its analogues[8b,c] is that the oxo ligand usually retains terminal coordination, and further coordination to other transition metal ions has not been reported so far. In this paper we present the synthesis of new coordination polymers and clusters prepared by attaching Mn^{II} to the terminal oxo ligands which have unprecedented molecular and supramolecular structures.

To date, most Mo(W)−M′−S (M′ = other transition metals) clusters have been synthesized via traditional solution reactions. The reactions usually involve thiometalates $[MO_{(4-n)}S_n]^{2-}$ (M = Mo, W; n = 2,3,4) and $M'L_n$ (L = Cl, Br, I, CN, SCN, etc.) and sometimes organic ligands. Over 200 clusters with a variety of different structures have been obtained by this route.[8] However, this approach has been so successful that it is increasingly difficult to synthesize new clusters with novel structures using this method, and new synthetic pathways and strategies need to be developed.

In this paper we present a new approach specifically targeting the rational assembly of polymetallic clusters containing more than one type of metal by the reaction of Mo−S−O-based clusters with oxophilic transition metal ions, in which the terminal oxo ligand attached to Mo binds Mn^{II}, with incorporation of multidentate organic ligands. Thus, a new class of organic−inorganic hybrid clusters has been produced by the combination of an Mo−S−O-based cluster with the relatively hard Mn^{II}.

Scheme 1. Proposed Pathway for the Conversion of **2** into **3**

$$[Mo^{(VI)}O_4]^{2-} \xrightarrow{(i)} [Mo^{(VI)}O_2S_2]^{2-} \xrightarrow{(ii)} [Mo^{(V)}{}_2O_2S_2edt_2]^{2-}$$

[a] Conditions: (i) H_2S, 5 min. (ii) $Na_2S_2O_4$, HS-CH_2-CH_2-SH, 90 °C, 2 hours.

Previous studies[14] have demonstrated that the thiol and bridging sulfur ligands of $[Mo_2O_2S_2(edt)_2]^{2-}$ act as μ- and μ_3-bridging ligands coordinated to some relatively soft Lewis acid ions, such as Cu^+ or Ag^+, resulting in a series of heterobimetallic dodecanuclear Mo^V/M'^I (M′ = Cu, Ag) cagelike clusters in which the oxo ligand on the Mo site retains terminal coordination. In addition, the terminal oxo ligand of these cage clusters further binds to alkali metal cations in the presence of dibenzo-18-crown-6, forming double-cage large clusters.[15] These observations led to our investigating the reaction of oxophilic transition metal cations [such as Mn^{2+}, Fe^{3+}, Co^{2+}, and Ni^{2+}] with $[Mo^V{}_2O_2S_2(edt)_2]^{2-}$ to understand whether the oxo ligand on $[MoV_2O_2S_2(edt)_2]^{2-}$ binds to these cations. As a relatively hard Lewis acid, Mn^{2+} prefers to be coordinated by oxygen and nitrogen donors rather than sulfur donors. Therefore, we selected Mn^{2+} as the first candidate in our approach.

Results and Discussion

Synthetic Strategies. $[NEt_4]_2[Mo^V{}_2O_2S_2(edt)_2]$ was synthesized as described previously.[14b] Although this complex has been used in the preparation of Mo^V/M'^I (M′ = Cu, Ag) cagelike clusters before,[14] the mechanism of $[NEt_4]_2[Mo_2O_2S_2(edt)_2]$ synthesis has not been discussed. Gaseous H_2S is bubbled into an aqueous solution of Na_2MoO_4 to form $[Mo^{VI}O_2S_2]^{2-}$. Subsequently, Mo^{VI} is reduced to Mo^V in the presence of $Na_2[S_2O_4]$ and 1,2-ethanedithiol (Scheme 1). Whether this is a one-electron reduction ($Mo^{VI} \rightarrow Mo^V$), or a two-electron reduction ($Mo^{VI} \rightarrow Mo^{IV}$) followed by a conproportionation ($Mo^{IV} + Mo^{VI} \rightarrow 2\ Mo^V$), as proposed for the induced internal electron transfer in the system $[MoS_4]^{2-}/R_2S_2 \rightarrow [\{SMo^V(S_2)\}_2]^{2-}$,[10b] is unclear. Both $Na_2[S_2O_4]$ and 1,2-ethanedithiol can be reductants. However, it seems likely that $Na_2[S_2O_4]$ is the dominant reductant since, if $Na_2[S_2O_4]$ is not added to the reaction mixture, the yield of $[NEt_4]_2[Mo_2O_2S_2(edt)_2]$ is low (less than 10%). $[NEt_4]_2[Mo_2O_2S_2(edt)_2]$ appears as the product in Scheme 1 and as reactant in the synthetic Scheme 2.

Many kinetic studies on Mn^{II} complexes have established the rapid substitution lability of Mn^{II} complexes.[16] It seems reasonable to propose that in solution Mn^{II} will bind to $[Mo_2O_2S_2(edt)_2]^{2-}$, producing cluster units of $[(MnL_y)\{Mo_2O_2S_2(edt)_2\}_x]^{n-}$ (L = solvent ligand; y = 5, x = 1, n =

(7) (a) Müller, A.; Diemann, E.; Jostes, R.; Bögge, H. *Angew. Chem., Int. Ed. Engl.* **1981**, *20*, 934. (b) Müller, A.; Dartmann, M.; Römer, C.; Clegg, W.; Sheldrick, G. M. *Angew. Chem., Int. Ed. Engl.* **1981**, *20*, 1060. (c) Du, S.-W.; Zhu, N.-Y.; Chen, P.-C.; Wu, X.-T. *Angew. Chem., Int. Ed. Engl.* **1992**, *31*, 1085. (d) Guo, J.; Wu, X.-T.; Zhang, W.-J.; Sheng, T.-L.; Huang, Q.; Lin, P.; Wang, Q.-M.; Lu, J.-X. *Angew. Chem., Int. Ed. Engl.* **1997**, *36*, 2464. (e) Lang, J.-P.; Kawaguchi, H.; Ohnishi, S.; Tatsumi, K. *Chem. Commun*. **1997**, 405.

(8) (a) Niu, Y.-Y.; Zheng, H.-G.; Hou, H.-W.; Xin, X.-Q. *Coord. Chem. Rev.* **2004**, *248*, 169. (b) Zhang, C.; Jin, G.-C.; Chen, J.-X.; Xin, X.-Q.; Qian, K.-P. *Coord. Chem. Rev.* **2001**, *213*, 51. (c) Hou, H.-W.; Xin, X.-Q.; Shi, S. *Coord. Chem. Rev.* **1996**, *153*, 25, and references therein.

(9) (a) Coucouvanis, D. *Adv. Inorg. Chem.* **1998**, *45*, 1. (b) Malinak, S. M.; Coucouvanis, D. *Prog. Inorg. Chem.* **2001**, *49*, 599. (c) Zhang, Y.; Holm, R. H. *J. Am. Chem. Soc.* **2003**, *125*, 3910. (d) Zhou, H.-C.; Su, W.-P.; Achim, C.; Rao, P. V.; Holm, R. H. *Inorg. Chem.* **2002**, *41*, 3191. (e) Huang, J.-S.; Mukerjee, S.; Segal, B. M.; Akashi, H.; Zhou, J.; Holm, R. H. *J. Am. Chem. Soc.* **1997**, *119*, 8662. (f) Demadis, K. D.; Campana, C. F.; Coucouvanis, D. *J. Am. Chem. Soc.* **1995**, *117*, 7832.

(10) (a) Simhon, E. D.; Baenziger, N. C.; Kanatzidis, M.; Draganjic, M.; Coucouvanis, D. *J. Am. Chem. Soc.* **1981**, *103*, 1218. (b) Coyle, C. L.; Harmer, M. A.; George, G. N.; Daage, M.; Stiefel, E. I. *Inorg. Chem.* **1990**, *29*, 14. (c) Bell, J.; Dunford, A. J.; Hollis, E.; Henderson, R. A. *Angew. Chem., Int. Ed.* **2003**, *42*, 1149. (d) Cui, Z.; Henderson, R. A. *Inorg. Chem.* **2002**, *41*, 4158.

(11) (a) Stiefel, E. I.; Matsumoto, K. *Transition Metal Sulfur Chemistry, Biological and Industrial Significance*; American Chemical Society: Washington, D.C., 1996; Chapter 17, pp 282−296. (b) Cianelli, R. R. *Catal. Rev.−Sci. Eng.* **1984**, *26*, 361.

(12) (a) Chen, L.; Wu, X.-T.; Gao, X.-C.; Zhang, W.-J.; Lin, P. *J. Chem. Soc., Dalton Trans.* **1999**, 4303. (b) Chen, L.; Yu, H.; Wu, L.-M.; Du, W.-X.; Gao, X.-C.; Lin, P.; Zhang, W.-J.; Cui, C.-P.; Wu, X.-T. *J. Solid State Chem.* **2000**, *151*, 286.

(13) (a) Shi, S.; Ji, W.; Tang, S.-H.; Lang, J.-P.; Xin, X.-Q. *J. Am. Chem. Soc.* **1994**, *116*, 3615. (b) Zhang, Q.-F.; Niu, Y.-Y.; Leung, Wa. H.; Song, Y.-L.; Williams, I. D.; Xin, X.-Q. *Chem. Commun*. **2001**, 1126.

(14) (a)Lin, P.; Wu, X.-T.; Zhang, W.-J.; Guo, J.; Sheng, T.-L.; Wang, Q.-M.; Lu, J.-X. *Chem. Commun*. **1997**, 1349. (b) Lin, P.; Wu, X.-T.; Huang, Q.; Wang, Q.-M.; Sheng, T.-L.; Zhang, W.-J.; Guo, J.; Lu, J.-X. *Inorg. Chem.* **1998**, *37*, 5672. (c) Lin, P.; Wu, X.-T.; Chen, L.; Wu, L.-M.; Du, W.-X. *Polyhedron* **2000**, *19*, 2189.

(15) Lin, P.; Clegg, W.; Harrington, R. W.; Henderson, R. A. *J. Chem. Soc., Dalton Trans.* **2005**, 2349.

(16) Tobe, M. L.; Burgess, J. *Inorganic Reaction Mechanisms*; Longman: Harlow, U.K., 1999; Chapter 7.

Scheme 2. Synthesis compounds **1**−**6**

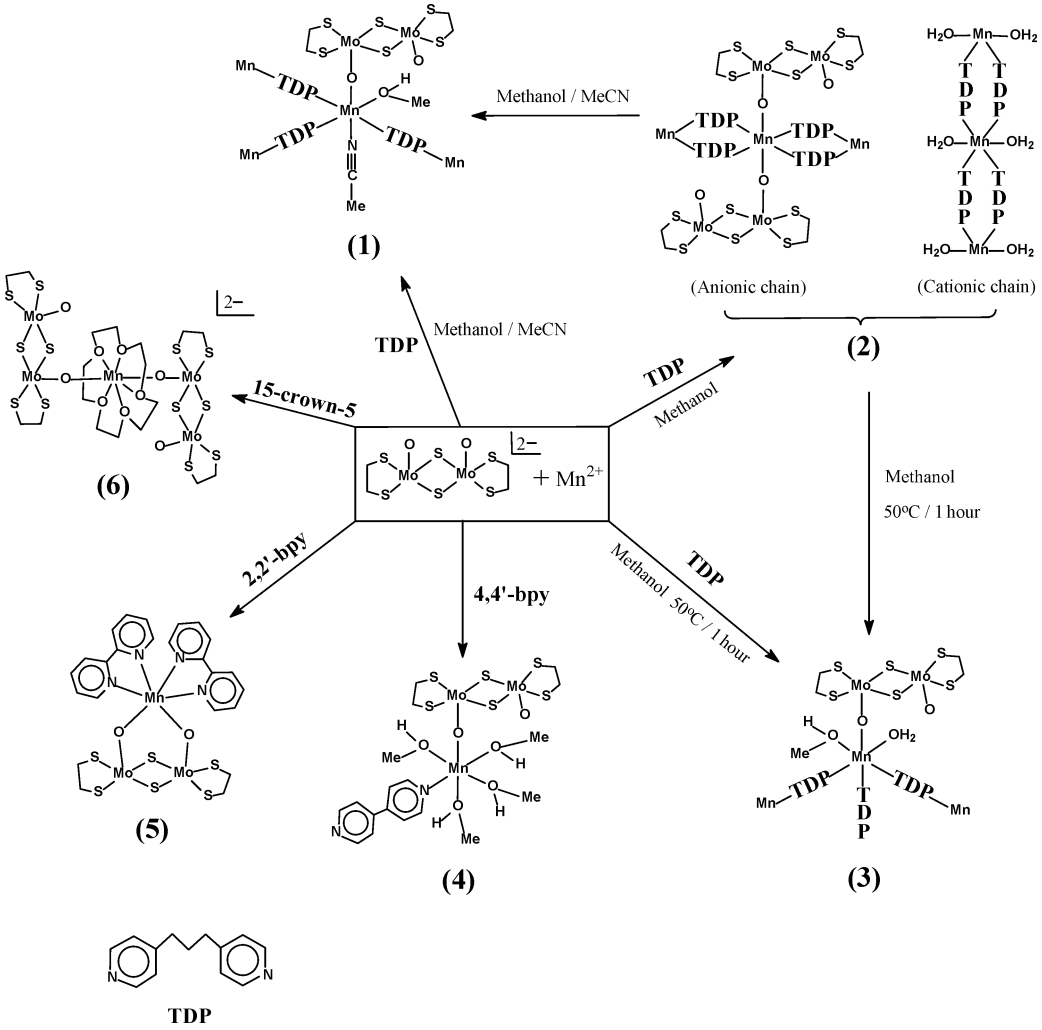

0; $y = 4$, $x = 2$, $n = 2$). Since only the oxo groups in $[Mo_2O_2S_2(edt)_2]^{2-}$ are terminal ligands, the Mn^{II} will coordinate only through the oxo ligands while the thiol and sulfide ligands remain unperturbed. For the putative $[(MnL_y)\{Mo_2O_2S_2(edt)_2\}_x]^{n-}$ (L = solvent) species, single crystals suitable for X−ray characterization are difficult to obtain due to the lability of the solvent ligands and high solubility of salts of $[(MnL_y)\{Mo_2O_2S_2(edt)_2\}_x]^{n-}$. Since $[Mo_2O_2S_2(edt)_2]^{2-}$ is inert to substitution, it is anticipated that multidentate ligands added to the reaction mixture will bind to the Mn^{II} because of the dynamic and labile coordination chemistry of this ion. Using this derivatization approach, it was possible to crystallize coordination polymers or discrete heterometallic cluster compounds containing the $[Mn\{Mo_2O_2S_2(edt)_2\}_x]^{2-2x}$ fragment.

The synthesis of compounds **1**−**6** was carried out under mild conditions, as indicated in Scheme 2. The solid-state structures of compounds **1**−**3** are cluster coordination polymers, while compounds **4**−**6** adopt discrete multinuclear cluster structures. Interestingly, the reaction of $Mn(NO_3)_2 \cdot 6H_2O$ with $[NEt_4]_2[Mo_2O_2S_2(edt)_2]$, at room temperature, in the presence of 2 molar equivalents of 4,4′-trimethylenedipyridine (TDP) in methanol/acetonitrile mixed solvent yields orange cuboid crystals of $[Mn_2\{Mo_2O_2S_2(edt)_2\}_2(TDP)_3(CH_3OH)_2(NCMe)_2] \cdot 3CH_3OH \cdot 0.25MeCN$ (**1**). However, when the reaction is carried out in methanol at room temperature, orange prismatic crystals of $[Mn(TDP)_2(H_2O)_2]^{2+}[Mn\{Mo_2O_2S_2(edt)_2\}_2(TDP)_2]^{2-} \cdot 6CH_3OH$ (**2**) are obtained, while the same reaction, carried out in hot methanol, results in yellow octahedral crystals of $[Mn\{Mo_2O_2S_2(edt)_2\}(TDP)_2(CH_3OH)(H_2O)] \cdot CH_3OH$ (**3**), which adopts a different structural configuration than that of **2**. The subtly different structures obtained in these reactions are discernible only by X-ray crystallography. In the following sections, we will initially present the structures of compounds **1**−**6** and subsequently discuss the conversions among **1**, **2**, and **3**.

Some General Structural Considerations. There are some general features of $[Mo_2O_2S_2(edt)_2]^{2-}$ which it is anticipated would control the structure of coordination polymers. These features are worth outlining before we discuss the structures of the compounds containing $[Mn\{Mo_2O_2S_2(edt)_2\}_x]^{2-2x}$ fragments.

It is known that bulky ligands [such as 1,3,5-tris(diphenylphosphanyl)benzene] can prevent polymeric frameworks forming interpenetrating and compact stacking within crystals.[17] This is because, to interpenetrate, the size of the vertex or diameter of the polymer strand must be less than the size of the cavity. Thus, the reaction of 1,3,5-tris(diphenyl-

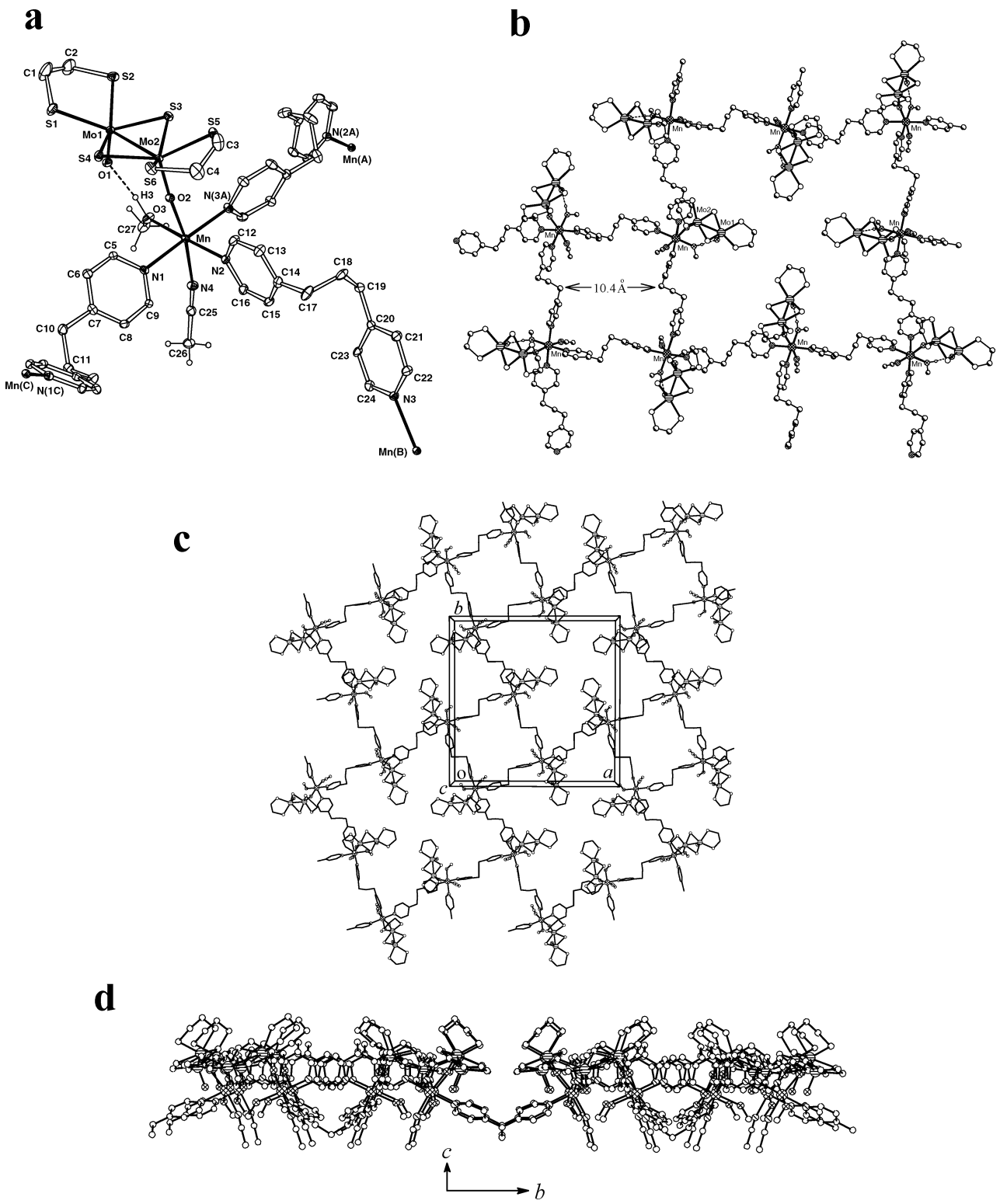

Figure 1. (a) Structure of [Mn{$Mo_2O_2S_2$(edt)$_2$}(NCMe)(MeOH)] in **1** and the bridging TDP ligands (30% displacement ellipsoids). The dotted line indicates an intramolecular hydrogen bond. Hydrogen atoms of TDP and edt ligands are omitted. For the sake of clarity, only the Mn centers of symmetry-related cluster units are shown. (b) The two types of square grids in **1**. Hydrogen atoms on carbon atoms are omitted. (c) A sheet of the extended two-dimensional network of **1** viewed down the crystallographic *c* axis. Hydrogen atoms are omitted. (d) The side view of one sheet of the two-dimensional network of **1**. The view is down the crystallographic *a* axis and includes the same atoms as shown in (c).

phosphanyl)benzene with $Ag(O_3SCF_3)$ (O_3SCF_3 = trifluoromethanesulfonate) produces a network polymer [Ag_4{1,3,5-tris(diphenylphosphanyl)benzene}$_3(O_3SCF_3)_4$].[17] However, this is a non-interpenetrating network because of the steric bulk of the ligand. It seems reasonable that [$Mo_2O_2S_2$(edt)2]2− would also be too bulky to allow interpenetrating polymeric frameworks and would hence give rise to cavities.

(17) Xu, X.-L.; Nieuwenhuyzen, M.; James, S. L. *Angew. Chem., Int. Ed.* **2002**, *41*, 764.

The two terminal oxo groups in $[Mo_2O_2S_2(edt)_2]^{2-}$ are syn to one another. Thus, polymeric networks comprising oxophilic transition metal cations and $[Mo_2O_2S_2(edt)_2]^{2-}$ could contain nodes of the transition metals at which two or more $[Mo_2O_2S_2(edt)_2]^{2-}$ units could link.

Structure of 1. The building block of **1** has an asymmetric configuration, as shown in Figure 1a. It contains [Mn{$Mo_2O_2S_2(edt)_2$}(MeOH)(NCMe)] units with three TDP ligands bound to Mn. The Mn site has a distorted octahedral geometry with one oxo ligand of $[Mo_2O_2S_2(edt)_2]$ bound at one axial site [Mn−O(2), 2.201(4) Å] and one acetonitrile molecule bound trans to this oxo ligand via the nitrogen atom [Mn−N(4), 2.286(4) Å]. The equatorial sites are occupied by one methanol [Mn−O(3), 2.201(4) Å] and three nitrogen atoms [N(1), N(2), and N(3A)] from three TDP ligands. The TDP ligands necessarily form a meridional arrangement at the Mn center. The O(2) atom bridges the $[Mo_2O_2S_2(edt)_2]^{2-}$ subunit and the Mn atom, forming an Mo−O−Mn bridge (Mo−O−Mn angle =165.1(2)°). The angles O(2)−Mn−N(4) and Mn−N(4)−C(25) are 169.73(15)° and 167.6(4)°, respectively.

The $[Mo_2O_2S_2(edt)_2]^{2-}$ subunit comprises two Mo^V centers bridged by two sulfur atoms and chelated by two 1,2-ethanedithiolate ligands, with an Mo−Mo bond distance of 2.8665(7) Å, comparable to those in $[NEt_4]_2[Mo_2S_4(edt)_2]$ (Mo−Mo = 2.863 Å)[18] and $[NBu_4]_2[Mo_2O_2S_2(S_2C_2(CN)_2)_2]$ (Mo−Mo = 2.821 Å).[19] Each Mo center has square-based pyramidal coordination geometry with one oxygen atom occupying the apical position. The four sulfur atoms in the basal plane are essentially coplanar. Each Mo is displaced from the basal plane toward the axial oxygen ligand, the deviation being 0.69 Å for Mo(1) and 0.70 Å for Mo(2). The Mo−O bond distances [1.720(3) and 1.728(3) Å] are slightly longer than those in $[NBu_4]_2[Mo_2O_2S_2(S_2C_2(CN)_2)_2]$ (1.661 and 1.666 Å).[19]

In **1**, an intramolecular O···H−O hydrogen bond exists between the terminal oxygen atom [O(1)] and the coordinated methanol molecule. This hydrogen-bonding interaction may afford additional stability and rigidity for the [Mn{$Mo_2O_2S_2(edt)_2$}(MeOH)(NCMe)] unit. Selected bond distances and angles, including the hydrogen bonding parameters for **1**, are listed in Table 1.

Each TDP ligand in **1** connects two Mn atoms, giving a two-dimensional network comprising two kinds of grid units. As shown in Figure 1b, the small grid unit consists of four [Mn{$Mo_2O_2S_2(edt)_2$}(CH_3OH)(NCMe)] cluster units linked by four TDP bridges, the Mn···Mn separation being 12.4 Å and the inner cavity dimensions ca. 10.4 Å × 10.4 Å (measured as the distances between the two closest carbon atoms opposite the TDP bridges). The large grid unit consists of eight [Mn{$Mo_2O_2S_2(edt)_2$}(CH_3OH)(NCMe)] cluster units connected by eight TDP bridges; every edge of this grid contains two linear TDP bridges, of which one is shared by the small grid as its edge. For each large grid unit, the four

Table 1. Selected Bond Distances (Å) and Angles (deg) for [Mn{$Mo_2O_2S_2(edt)_2$}$(TDP)_{1.5}$(MeOH)(NCMe)]·1.5MeOH·0.125MeCN (**1**)[a]

Mo(1)−Mo(2)	2.8665(7)	Mo(1)−S(1)	2.4316(16)
Mo(1)−S(2)	2.4217(15)	Mo(1)−S(3)	2.3363(14)
Mo(1)−S(4)	2.3488(14)	Mo(1)−O(1)	1.720(3)
Mo(2)−S(3)	2.3365(14)	Mo(2)−S(4)	2.3368(14)
Mo(2)−S(5)	2.4219(14)	Mo(2)−S(6)	2.4205(15)
Mo(2)−O(2)	1.728(3)	Mn−O(2)	2.192(3)
Mn−O(3)	2.201(4)	Mn−N(1)	2.252(4)
Mn−N(2)	2.272(4)	Mn−N(3A)	2.257(4)
Mn−N(4)	2.286(4)	N(3)−Mn(B)	2.257(4)
Mo(2)−O(2)-Mn	165.1(2)	O(2)−Mn−N(4)	169.73(15)
O(2)−Mn−O(3)	88.95(13)	N(1)−Mn−N(4)	86.30(15)
N(2)−Mn−N(4)	91.20(16)	N(3A)−Mn−N(4)	95.00(16)
Mn−O(3)−C(27)	130.3(3)	Mn−N(4)−C(25)	167.6(4)

Hydrogen Bond Distances and Angles for **1**

D−H···A	*d*(D−H)	*d*(H···A)	*d*(D···A)	∠(DHA)
O(3)−H(3)···O(1)	0.98(2)	1.78(2)	2.752(5)	173(5)

[a] Symmetry operations for equivalent atoms: A, (y, 1/2 − x, z); B, (1/2 − y, x, z); C, (1/2 − x, 3/2 − y, z).

$[Mo_2O_2S_2(edt)_2]$ subunits are regularly oriented toward the center of the large grid, resulting in an incomplete open cavity.

Figure 1c shows a single sheet of the extended two-dimensional structure in **1**. In the sheet, each large grid shares edges with four outer small grids and four outer large grids in such a way that each small grid is surrounded by four large grids and shares four-half-edges from the four large grids. Within the sheet, all Mn atoms are exactly coplanar, with all of the bonded MeCN ligands located on the same side of, and perpendicular to, the plane of the Mn centers. All $[Mo_2O_2S_2(edt)_2]$ subunits are located on the opposite side of the plane to that of the MeCN ligands (Figure 1d).

The X-ray crystal structure reveals that **1** has an unusual double-sheet architecture. A schematic view of one double-sheet structure of **1** is shown in Figure 2a. The double-sheet structure comprises two symmetry-related two-dimensional sheets. The double-sheet network is non-interpenetrating, and the square grids from the two sheets stack on top of each other in a staggered arrangement. It is important to appreciate that there are no covalent interactions between the two sheets. Interestingly, the two sheets are stacked very closely, so that the two planes defined by the Mn atoms from each of the sheets have a perpendicular separation of 0.85 Å, and the small grids are positioned in the incomplete open cavities of the larger grids of the adjacent sheet. Figure 2b shows the partial structure of this double-sheet architecture (hereafter referred to as unit **C**), which contains a large square grid unit of $[Mn\{Mo_2O_2S_2(edt)_2\}(TDP)(MeOH)(NCMe)]_8$ (unit **B**) and one small square grid unit of $[Mn\{Mo_2O_2S_2(edt)_2\}(TDP)(MeOH)(NCMe)]_4$ (unit **A**) from the next sheet.

As shown in Figure 2c, unit **C** can be viewed as an assembly which comprises unit **A** incompletely intercalated into unit **B** (like a plug inserted into its socket). The acetonitrile ligands associated with unit **A** are completely embedded in the cavity of unit **B**. Such a structure is unprecedented in coordination polymer systems.

Although there are no covalent interactions between adjacent sheets in **1**, there are a significant number of van

(18) Bunzey, G.; Enemark, J. H. *Inorg. Chem.* **1978**, *17*, 682.
(19) Gelder, J. I.; Enemark, J. H. *Inorg. Chem.* **1976**, *15*, 1839.

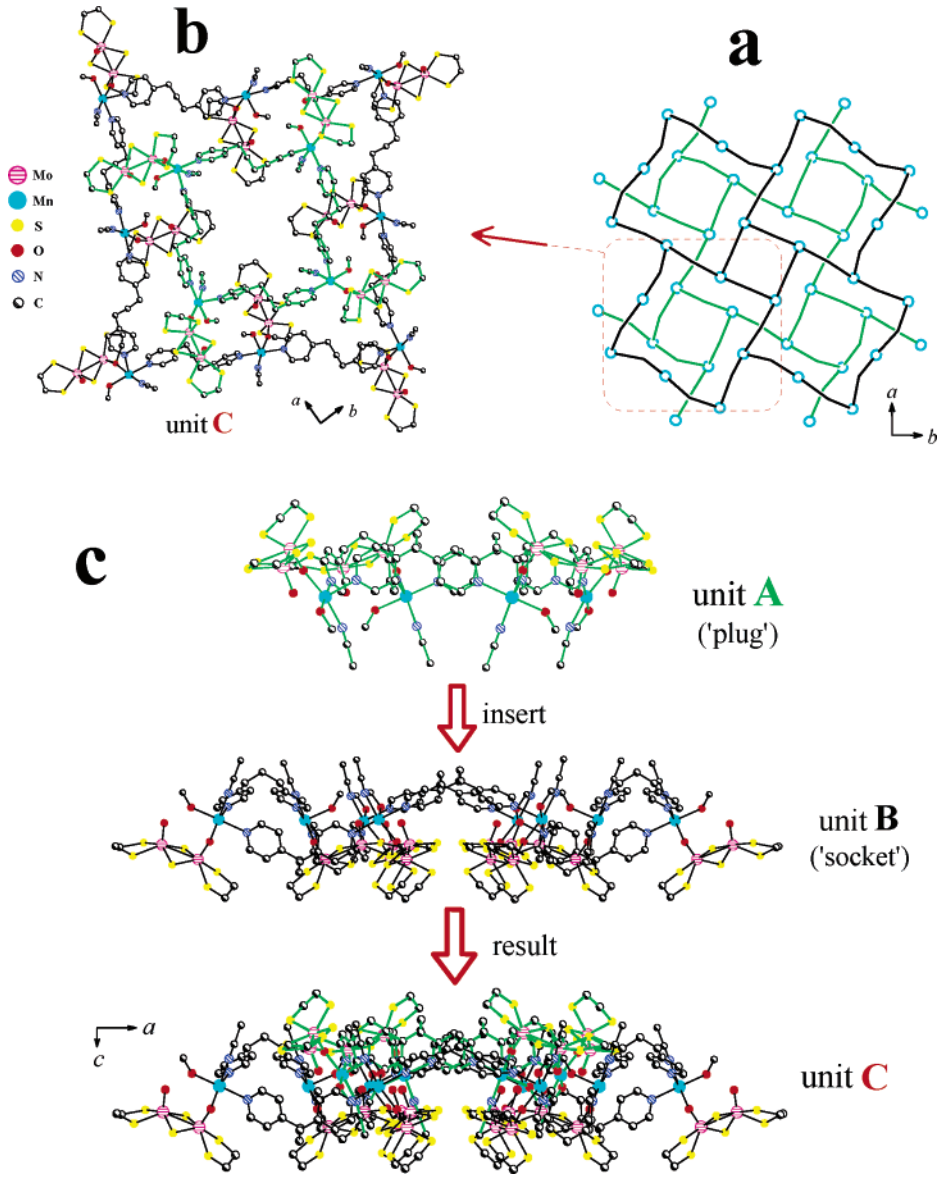

Figure 2. (a) Schematic view of the non-interconnected double-sheet structure in **1**. The view is along the crystallographic *c* axis. Every blue circle represents a $[Mn\{Mo_2O_2S_2(edt)_2\}(MeOH)(NCMe)]$ cluster unit. The black and green lines represent the TDP bridges from two adjacent sheets. (b) The structure of the **C** unit in **1** which consists of a large square grid unit of $[Mn\{Mo_2O_2S_2(edt)_2\}(TDP)(MeOH)(NCMe)]_8$ (unit **B**, the bonds are shown in black) and one small square grid unit of $[Mn\{Mo_2O_2S_2(edt)_2\}(TDP)(MeOH)(NCMe)]_4$ (unit **A**, the bonds are shown in green) from the adjacent sheet. The view is along the crystallographic *c* axis. Hydrogen atoms are omitted for clarity. (c) View of the **C** unit (including the same atoms as shown in (b)) down the crystallographic *b* axis, showing how the units (**A** and **B**) are used to construct unit **C**.

der Waals interactions present between adjacent sheets in the double-sheet architecture. These are C···S van der Waals interactions involving both the carbon atoms of MeCN ligands and the sulfur atoms of the edt ligands (distances range from 3.4 to 3.7 Å). Presumably, these weak intermolecular interactions contribute to the stabilization of the double-sheet structure.

Bilayer motifs such as the double-sheet structure observed for **1** are rare for coordination polymers. Compound **1** differs from the reported examples of bilayer structures.[5d,20,21] In the compounds reported so far, bridging covalent linkers connect adjacent sheets to form a bilayer structure.[5d,20,21] Therefore, the polymeric backbone of **1** represents a novel two-dimensional framework for coordination polymer systems.

We anticipate that the grid units in **1** can be slightly distorted because (i) the TDP molecule has a long and flexible $-(CH_2)_3-$ tether group linking its two pyridine groups and (ii) there are no direct connections between adjacent sheets. Such versatility in cavity size could lead to the double−sheet layer expanding and changing its internal cavity and raises the possibility of introducing small guest

(20) Hennigar, T. L.; MacQuarrie, D. C.; Losier, P.; Roger, R. D.; Zaworotko, M. J. *Angew. Chem., Int. Ed. Engl.* **1997**, *36*, 972. (b) Power, K. N.; Hennigar, T. L.; Zaworotko, M. J. *New. J. Chem.* **1998**, 177. (c) Carluci, L.; Ciani, G.; Proserpio, D. M.; Sironi, A. *Angew. Chem., Int. Ed. Engl.* **1995**, *34*, 1895.

(21) (a) Fu, Z.-Y.; Wu, X.-T.; Dai, J.-C.; Wu, L.-M.; Cui, C.-P.; Hu, S.-M. *Chem. Commun.* **2001**, 1856. (b) Hill, R. J.; Long, D.-L.; Turvey, M.-S.; Blake, A. J. Champness, N. R., Hubbersty, P.; Wilson, C.; Schröder, M. *Chem. Commun.* **2004**, 1792.

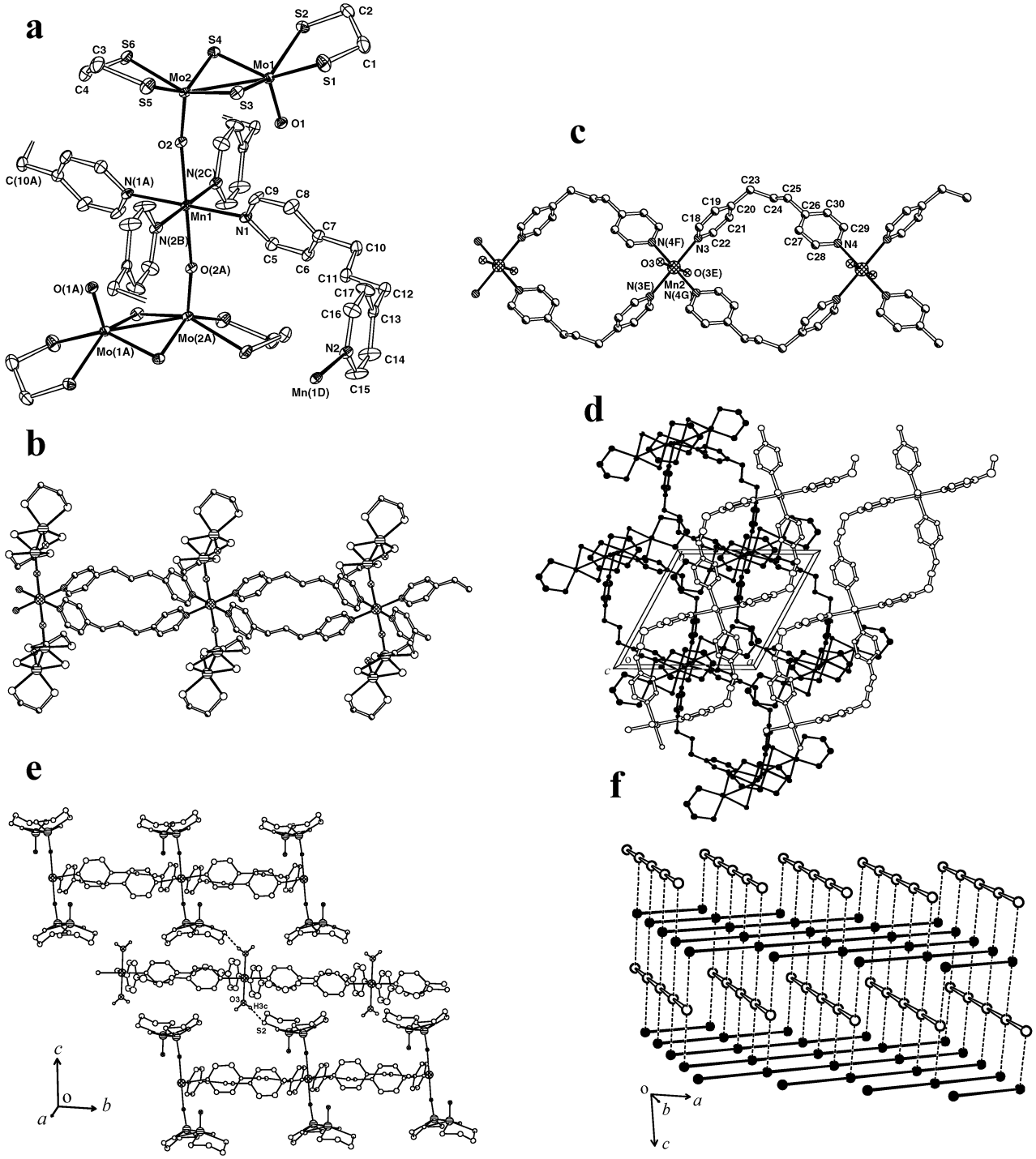

Figure 3. (a) Structure of the $[Mn\{Mo_2O_2S_2(edt)_2\}_2]^{2-}$ fragment of the anionic polymer in **2** together with the associated TDP ligands (30% displacement ellipsoids). Hydrogen atoms on carbons are omitted. Only the non-hydrogen atoms of one TDP bridging ligand are shown for clarity. (b) View of the anionic one-dimensional polymer of $[\{Mn(Mo_2O_2S_2(edt)_2)_2(TDP)_2\}^{2-}]_n$ in **2** with hydrogen atoms omitted. (c) View of the cationic one-dimensional polymer of $[\{Mn(H_2O)_2(TDP)_2\}^{2+}]_n$ in **2**, showing the coordination mode for the Mn center and bridging TDP ligand. Hydrogen atoms are omitted. (d) Packing view of **2**, looking edge-on down the crystallographic *c* axis. This view shows two cationic chains (atoms and bonds represented by white circles and double line) within the same layer (halfway along the *c* axis and parallel to the *ab* plane) and two anionic chains (atoms and bonds are represented by black circles and thick lines) within a layer below the cationic chains. (e) A view showing O−H···S hydrogen bonding (dashed line) occurring between one cationic and one anionic chain. Hydrogen atoms on carbon atoms are omitted. (f) A schematic view of the structure of **2**, showing the alternating arrangement of cationic and anionic one-dimensional polymers and the slipped O−H···S hydrogen-bond connectivity (broken lines). The $[Mn\{Mo_2O_2S_2(edt)_2\}_2]^{2-}$ units are represented by black spheres, which are connected by black rods, corresponding to the anionic one-dimensional polymer. The $[Mn(H_2O)_2]^{2+}$ units is represented by white spheres, which are connected by white rods, corresponding to the cationic one-dimensional polymer.

molecules between layers, which has potential importance in supramolecular materials.[5f]

Structure of 2. Compound **2** contains both the cationic one-dimensional coordination polymer $[\{Mn(TDP)_2(H_2O)_2\}^{2+}]_n$ and the anionic one-dimensional cluster coordination polymer $[\{Mn(Mo_2O_2S_2(edt)_2)_2(TDP)_2\}^{2-}]_n$.

The structure of the basic unit of the anionic polymer is shown in Figure 3a. The six-coordinate Mn^{II} lies on a

Table 2. Selected Bond Distances (Å) and Angles (deg) for $[\{Mn(TDP)_2(H_2O)_2\}^{2+}\{Mn(Mo_2O_2S_2(edt)_2)_2(TDP)_2\}^{2-}]\cdot 6MeOH$ (**2**)[a]

Mo−S	2.3322(8)−2.4458(9)	Mo(1)−Mo(2)	2.8483(4)
Mo(1)−O(1)	1.686(2)	Mo(2)−O(2)	1.730(2)
Mn(1)−N(1)	2.241(3)	Mn(1)−N(1A)	2.241(3)
Mn(1)−N(2C)	2.304(2)	Mn(1)−N(2B)	2.304(2)
Mn(1)−O(2)	2.269(2)	N(2)−Mn(1D)	2.304(2)
Mn(2)−N(3)	2.309(4)	Mn(2)−N(3E)	2.309(4)
Mn(2)−N(4F)	2.21(4)	Mn(2)−N(4G)	2.21(4)
Mn(2)−O((3)	2.178(3)		
Mo(2)−O(2)-Mn(1)	171.06(12)	N(1)−Mn(1)−N(2B)	87.61(9)
N(1)−Mn(1)−N(2C)	92.39(9)	O(2)−Mn(1)−N(1)	92.88(9)
N(3)−Mn(2)−N(4F)	84.9(8)	N(3)−Mn(2)−N(4G)	95.1(4)
N(3)−Mn(2)−O(3)	91.00(13)		

Hydrogen Bond Distances and Angles

D−H···A	*d*(D−H)	*d*(H···A)	*d*(D···A)	∠(DHA)
O(3)−H(3c)···S(2)	0.901(18)	2.28(2)	3.173(3)	171(4)

[a] Symmetry operations for equivalent atoms: A, $(1-x, 2-y, -z)$; B, $(-x, 3-y, -z)$; C, $(1+x, -1+y, z)$; D, $(-1+x, 1+y, z)$; E, $(1-x, 1-y, 1-z)$; F, $(x, 1+y, z)$; G, $(1-x, -y, 1-z)$.

crystallographic inversion center and is ligated by four equatorial nitrogen atoms from four TDP ligands and two symmetry-related $[Mo_2O_2S_2(edt)_2]^{2-}$ subunits axially bound via two oxo ligands, one from each $[Mo_2O_2S_2(edt)_2]^{2-}$ [Mn(1)−O(2) = Mn(1)−O(2A), 2.269(2) Å; Mo(2)−O(2)−Mn(1), 171.06(12)°], giving a long Mo−O−Mn−O−Mo bridge in a nearly linear arrangement. The remaining oxo ligand of each $[Mo_2O_2S_2(edt)_2]$ subunit does not interact with Mn. Selected bond distances and angles are listed in Table 2. The Mn centers in the anionic polymer are linked by two TDP ligands to form a one-dimensional chain decorated by $[Mo_2O_2S_2(edt)_2]$ subunits on both sides of the chain (Figure 3b). The closest Mn···Mn intrachain distance is 12.7 Å. For each $[Mn\{Mo_2O_2S_2(edt)_2\}_2]$ fragment, the four Mo and one Mn atoms are exactly coplanar.

For the cationic 1-dimensional polymer $[\{Mn(TDP)_2(H_2O)_2\}^{2+}]_n$ in **2** (Figure 3c), the Mn^{II} sites are six-coordinate with two terminal water molecules in trans positions [Mn(2)−O(3) 2.178(3) Å] and four pyridyl groups in the equatorial sites. The TDP ligands link adjacent Mn atoms in a double-stranded bridge fashion, which results in a cationic one-dimensional infinite structure containing alternate $Mn_2(TDP)_2$ rings, producing a small cavity. The internal N−Mn−N angle of the ring [N(3)−Mn(2)−N(4G)] is 95.1°, which is larger than the corresponding internal N−Mn−N angle in the anionic chain [87.61(9)°]. Consequently, the closest Mn···Mn intrachain distance in the cationic polymer is 12.10 Å. This is somewhat shorter than that in the anionic chain (12.73 Å).

As shown in Figure 3d, the anionic chains of **2** extend along the crystallographic $[1\bar{1}0]$ direction, forming an anionic layer which is parallel to the crystallographic *ab* plane. The cationic chains extend along the *b* axis, forming a cationic layer adjacent to the anionic layer. The dihedral angle between the cationic and anionic chains is 58°. There is no interpenetration in the packing of the anionic and cationic polymeric chains. Weak intermolecular hydrogen bonds occur between one sulfur atom of the edt ligand in the anionic chain and the water molecule of the cationic chain, as shown in Figure 3e; the hydrogen-bonding parameters are presented in Table 2. Apart from the O−H···S hydrogen bonding, no specific interactions between the polymer chains are present. It is worth noting that each water ligand has one O−H bond not involved in hydrogen bonding. Presumably, the terminal oxo ligand of the $[Mn\{Mo_2O_2S_2(edt)_2\}_2]$ fragment of the anionic polymer is too sterically hindered to be involved in hydrogen bonding. Figure 3f is a schematic view of the solid-state structure of **2**, showing the interchain O−H···S hydrogen bonds connecting adjacent layers. The layers stack in an ABAB-type arrangement along the crystallographic *c* axis. Since the cationic chain is tilted with respect to the anionic chain, each cationic chain is only singly hydrogen bonded to each anionic chain.

Only one other compound, $[WS_4Cu_4(4,4'\text{-bipy})_4][WS_4Cu_4I_4(4,4'\text{-bipy})_2]$,[22] has been reported which contains both cationic and anionic coordination polymers. However, in this compound, the cationic and anionic coordination polymers interpenetrate, forming an intricate three-dimensional architecture.

Structure of 3. The structure of **3** is shown in Figure 4a. This is an $[Mn\{Mo_2O_2S_2(edt)_2\}(MeOH)(OH_2)]$ fragment ligated by TDP ligands, in which the local coordination geometry around the Mn^{II} is slightly distorted octahedral, being equatorially coordinated by one methanol molecule [Mn−O(4), 2.203(5) Å], one water molecule [Mn−O(3), 2.166(4) Å], and two nitrogen atoms [N(4), N(3A)] from two TDP molecules. The methanol and the water molecules are cis to one another. The axial positions of Mn are occupied by one nitrogen atom from a TDP molecule and one oxo ligand from the $[Mo_2O_2S_2(edt)_2]$ subunit, forming an Mo−O−Mn bridge with an angle of 153.0(2)°, which is significantly smaller than the corresponding Mo−O−Mn angle in compounds **1** [165.1(2)°] and **2** [171.06(12)°]. Selected bond distances and angles are listed in Table 3.

There is an intramolecular O···H−O hydrogen bond between the terminal oxygen atom [O(1)] and the coordinated water molecule [O(1)···O(3), O(1)···H(3d), O(1)···H(3)−O(3): 2.806(5) Å, 1.93(3) Å, 170(8)°]. A similar hydrogen bond is present in (**1**). The three TDP ligands in (**3**) are arranged in a *fac* arrangement at Mn with the N−Mn−N angles ranging from 88.69(16)° to 100.78(16)°. This is different from **1**, where the three TDP ligands form a *mer* arrangement. The two equatorially bonded TDP ligands in **3** bridge two Mn centers from adjacent $[Mn\{Mo_2O_2S_2(edt)_2\}(MeOH)(OH_2)]$ fragments, resulting in an undulating one-dimensional coordination polymer running along the crystallographic *b* axis (Figure 4b). In contrast, the axially bonded TDP ligand is only a monodentate ligand, with its remaining nitrogen donor [N(2)] uncoordinated. Within the coordination polymer, all Mn atoms lie exactly coplanar, parallel to the crystallographic *ab* plane, the monodentate TDP ligands being tilted toward this plane and projecting outward in two orientations.

In the crystal structure of **3**, strong interchain N···H−O hydrogen bonds occur between the coordinated water ligand

(22) Liang, K.; Zheng, H.-G.; Song, Y.-L.; Lappert, M. F.; Li, Y.-Z.; Xin, X.-Q.; Huang, Z.-X.; Chen, J.-T.; Lu, S.-F. *Angew. Chem., Int. Ed.* **2004**, *43*, 5776.

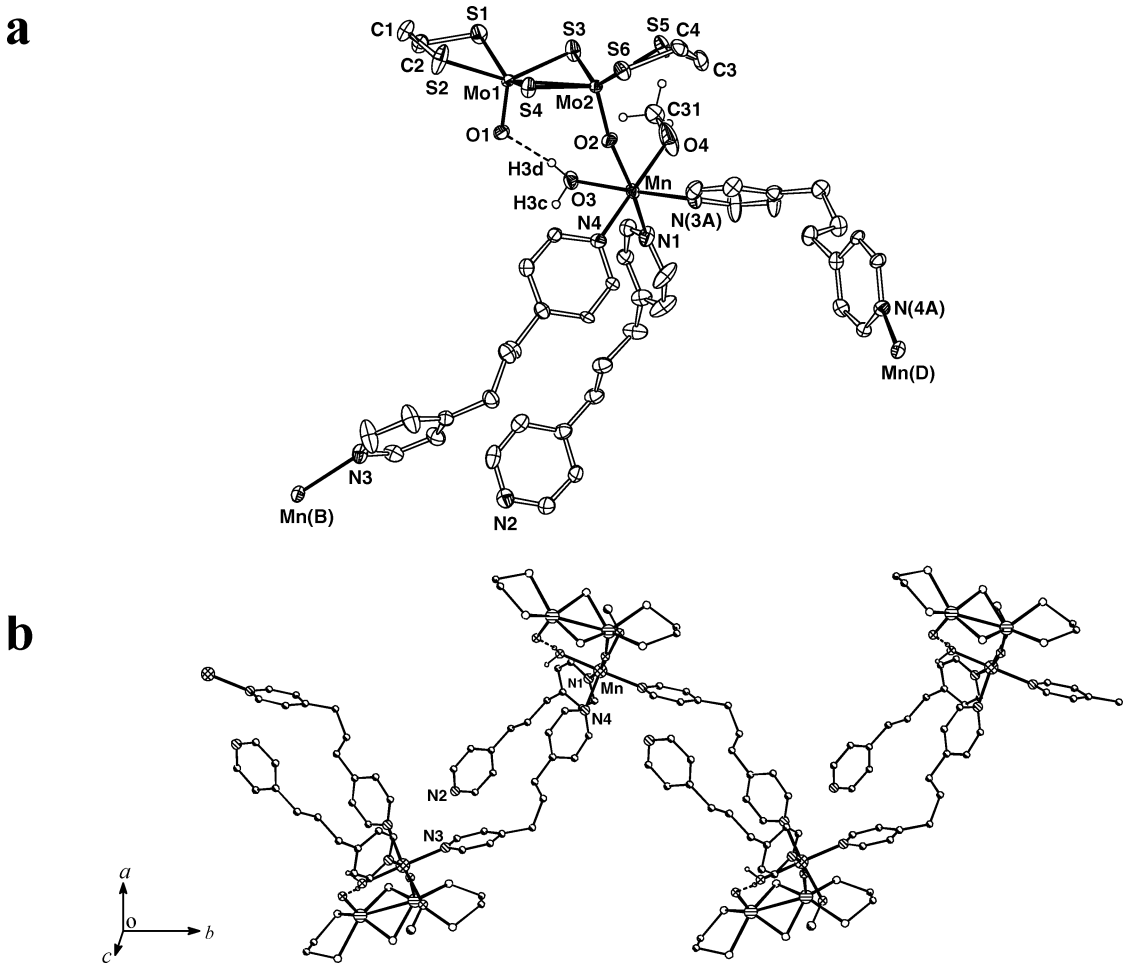

Figure 4. (a) Structure of the $[Mn\{Mo_2O_2S_2(edt)_2\}(OH_2)(MeOH)]$ unit in **3**, together with the associated TDP ligands (30% displacement ellipsoids). The dotted line indicates an intramolecular hydrogen bond. Hydrogen atoms of TDP and edt ligands are omitted. (b) Structure of the one-dimensional undulating chain of **3**. Hydrogen atoms on the carbon atoms are omitted for clarity.

Table 3. Selected Bond Distances (Å) and Angles (deg) for $[Mn\{Mo_2O_2S_2(edt)_2\}(TDP)_2(MeOH)(H_2O)]\cdot MeOH$ (**3**)[a]

Mo−S	2.3142(14)−2.4113(14)	Mo(1)−Mo(2)	2.8447(6)
Mo(1)−O(1)	1.700(3)	Mo(2)−O(2)	1.709(3)
Mn−N(1)	2.271(5)	Mn−N(4)	2.280(5)
Mn−N(3A)	2.228(4)	Mn−O(2)	2.192(4)
Mn−O(3)	2.166(4)	Mn−O(4)	2.203(5)
N(3)−Mn(B)	2.228(4)		
Mo(2)−O(2)−Mn	153.0(2)	O(2)−Mn−N(1)	168.18(16)
O(2)−Mn−O(3)	85.54(14)	O(2)−Mn−O(4)	87.1(2)
Mn−O(4)−C(31)	128.2(4)	N(1)−Mn−N(4)	98.33(17)
N(1)−Mn−N(3A)	100.78(16)	N(3A)−Mn−N(4)	88.69(16)
O(3)−Mn−O(4)	95.32(16)		

Hydrogen Bond Distances and Angles for **3**

D−H···A	*d*(D−H)	*d*(H···A)	*d*(D···A)	∠(DHA)
O(3)−H(3d)···O(1)	0.89(2)	1.93(3)	2.806(5)	170(8)
O(3)−H(3c)···N(2C)	0.89(2)	1.82(3)	2.693(6)	165(6)

[a] Symmetry operations for equivalent atoms: A, $(1/2 - x, 1/2 + y, 1/2 - z)$; B, $(1/2 - x, -1/2 + y, 1/2 - z)$; C, $(1 - x, -y, 1 - z)$; D, $(1/2 - x, 1/2 + y, 1/2 - z)$.

and the uncoordinated N(pyridyl) atom from adjacent chains in **3** (Figure 5a); details of the hydrogen bonding are given in Table 3. These interchain hydrogen bonds link adjacent one-dimensional coordination polymers, producing a two-dimensional network which contains elliptical rings supported by hydrogen bonds. Each ring comprises two Mn atoms, two bonded water molecules, and two monodentate TDP molecules from two adjacent polymeric chains. Within this two-dimensional framework, adjacent polymeric chains align in a staggered fashion and the rings alternately link adjacent polymeric chains along the *b* direction. One layer of **3**, formed by interchain hydrogen bonds linking one-dimensional cluster coordination polymers, is shown edge-on in Figure 5b. There are no major interactions between adjacent layers. For each Mn, one disordered methanol molecule is present in the crystal structure; this methanol does not form significant interactions with other molecules.

Structure of 4. To investigate the influence of the length of the organic linker on the structure of the material formed, the reaction between $Mn(NO_3)_2\cdot 6H_2O$ and $[Mo_2O_2S_2(edt)_2]^{2-}$ was performed with 4,4′-bipyridine (4,4′-bipy) present rather than TDP. The reaction at room temperature produced **4**, which X-ray crystallography shows is the discrete heterometallic cluster $[Mn\{Mo_2O_2S_2(edt)_2\}(4,4'\text{-bpy})(CH_3OH)_4]$, having half a molecule of uncoordinated 4,4′-bpy per dimer (Figure 6a). Mn is six-coordinate with three equatorial methanol ligands and one nitrogen atom [N(1)] from a monodentate 4,4′-bpy ligand. The fourth methanol ligand is bound to an axial site and the remaining axial position is occupied by one oxygen atom of an $[Mo_2O_2S_2(edt)_2]$ unit, forming an Mo−O−Mn bridge with an angle of 158.8(3)°.

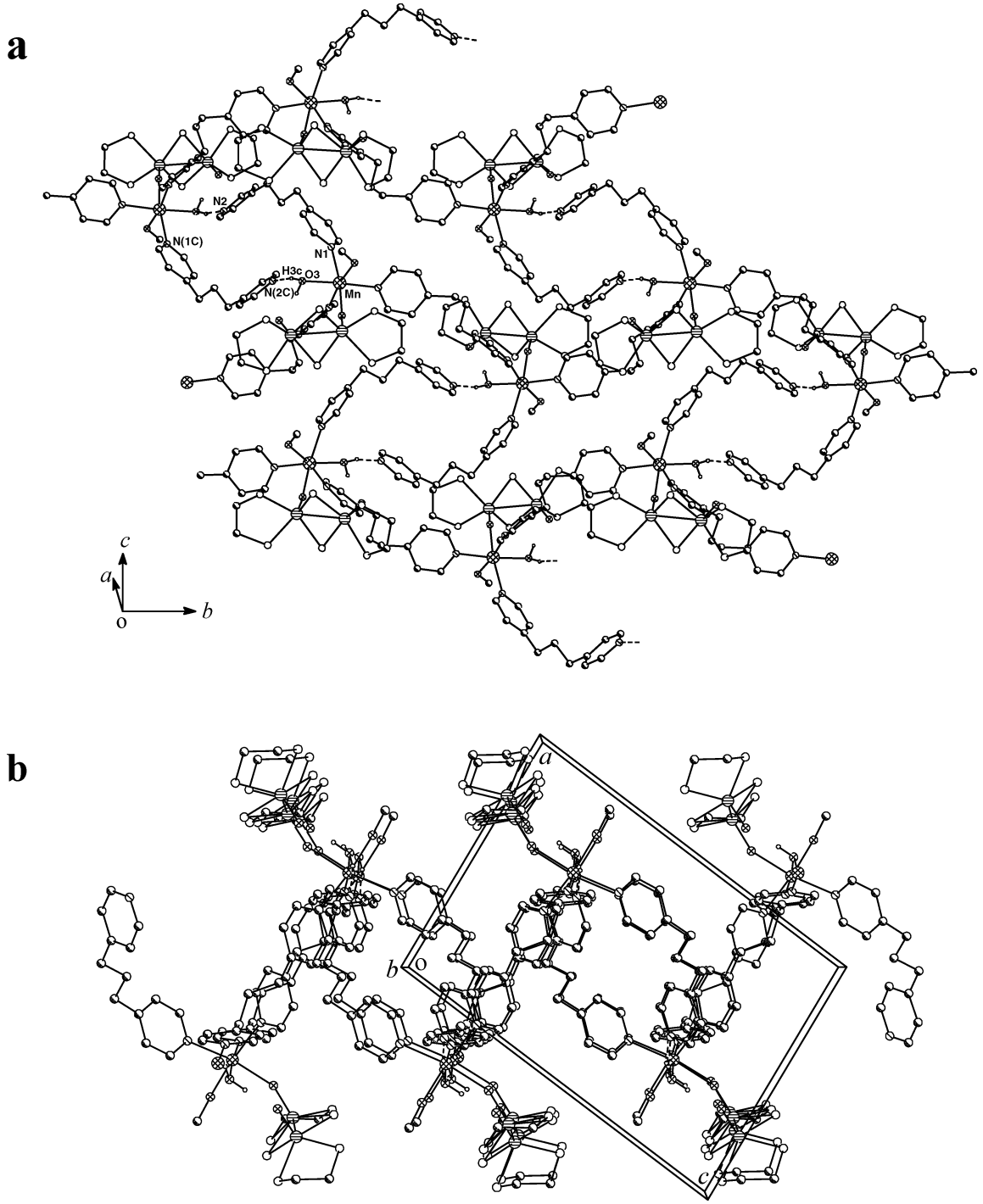

Figure 5. (a) Figure showing the two-dimensional sheet network in **3**, with the intermolecular hydrogen bonds between adjacent polymeric chains indicated as dashed lines. Hydrogen atoms on the carbon atoms are omitted for clarity. (b) A single layer of the hydrogen-bonded two-dimensional network in **3** viewed edge-on down the crystallographic *b* axis. The view includes the same atoms as shown in (a).

The two pyridine rings of the mono-coordinated 4,4′-bpy ligand are twisted by 38.1° with respect to each other. Selected bond distances and angles are given in Table 4.

Within $[Mo_2O_2S_2(edt)_2]$ in **4**, the terminal oxo ligand not bonded to Mn forms an intramolecular hydrogen bond to an equatorial methanol ligand [O(2)···O(4), 2.699(7) Å; O(2)···H(4)−O(4), 167(9)°]; a similar interaction is observed in **1** and **3**.

The pyridine rings of the centrosymmetric uncoordinated 4,4′-bpy molecule are exactly coplanar, and this ligand is hydrogen-bonded to one equatorial methanol ligand of the cluster unit via one nitrogen atom. In addition, $\pi\cdots\pi$ interactions (center to center, ca. 3.6 Å) occur between one pyridine ring [containing N(3)] of the uncoordinated 4,4′-bpy and one pyridine ring [containing N(1)] of the coordinated 4,4′-bpy ligand. The remaining pyridine rings from the two 4,4′-bpy molecules are separated (center to center) by about 4.6 Å, which is beyond the range (3.3−3.8 Å) normally associated with $\pi\cdots\pi$ interactions.[23] Figure 6b shows how each cluster unit interacts with adjacent sym-

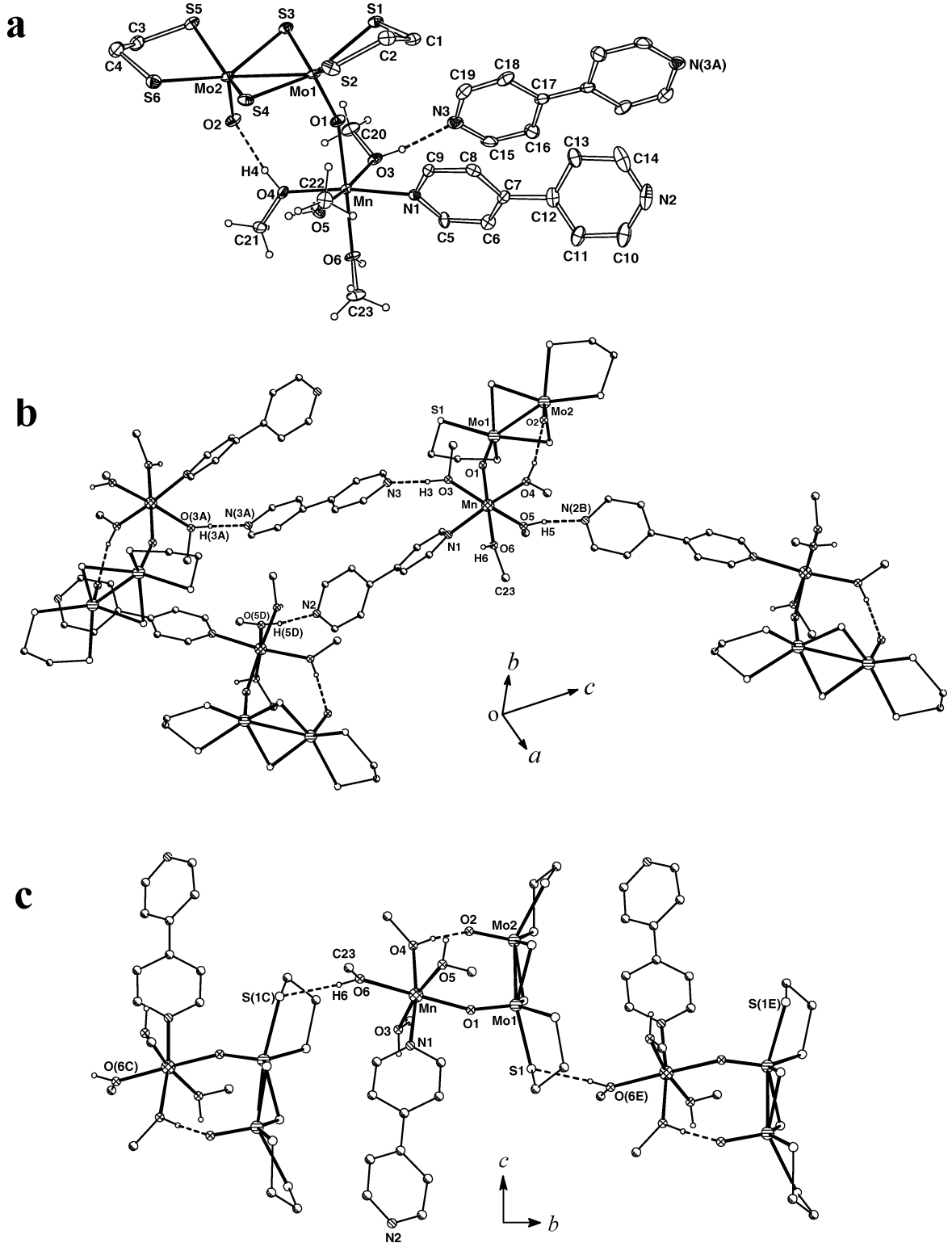

Figure 6. (a) Molecular structure of $[Mn\{Mo_2O_2S_2(edt)_2\}(4,4'\text{-bpy})(CH_3OH)_4]$ **4** showing the uncoordinated 4,4′-bipyridine (30% displacement ellipsoids). Hydrogen atoms (except for the methanol ligands) are omitted for clarity. (b) A view showing the hydrogen-bonded connectivity between adjacent cluster units and the uncoordinated 4,4′-bipyridine. Hydrogen atoms on the carbon atoms are omitted. For the sake of clarity, symmetry-related cluster units linked by O−H···S hydrogen bonds are not shown. (c) View of the symmetry-related cluster units linked by O−H···S hydrogen bonds in **4**.

metry-related cluster units and the uncoordinated 4,4′-bpy molecule through intermolecular O−H···N hydrogen-bond interactions.

In addition to the intermolecular hydrogen-bonding of the uncoordinated 4,4′-bpy molecule, the uncoordinated nitrogen atom [N(2)] of each monodentate 4,4′-bpy ligand also participates in intermolecular hydrogen bonding. Furthermore, there are intermolecular O−H···S hydrogen bonds

(23) Janiak, C. J. *J. Chem. Soc., Dalton Trans.* **2000**, 3885.

Table 4. Selected Bond Distances (Å) and Angles (deg) for $[Mn\{Mo_2O_2S_2(edt)_2\}(4,4'\text{-bpy})(CH_3OH)_4]\cdot 0.5(4,4'\text{-bpy})$ (**4**)

Mo−S	2.3211(19)−2.4433(19)	Mo(1)−Mo(2)	2.8554(9)
Mo(1)−O(1)	1.715(5)	Mo(2)−O(2)	1.703(5)
Mn−O(1)	2.172(5)	Mn−O(3)	2.172(5)
Mn−O(4)	2.158(5)	Mn−O(5)	2.131(5)
Mn−O(6)	2.203(5)	Mn−N(1)	2.202(6)
Mo(1)−O(1)−Mn	158.8(3)	O(1)−Mn−O(6)	177.25(19)
O(1)−Mn−N(1)	94.6(2)	Mn−O(3)−C(20)	119.8(5)
Mn−O(4)−C(21)	131.8(4)	Mn−O(5)−C(22)	136.3(5)
Mn−O(6)−C(23)	125.8(5)		

Hydrogen Bond Distances and Angles for **4**

D−H···A	*d*(D−H)	*d*(H···A)	*d*(D···A)	∠(DHA)
O(3)−H(3)···N(3)	0.89(2)	1.87(2)	2.755(9)	170(6)
O(4)−H(4)···O(2)	0.88(2)	1.83(2)	2.699(7)	167(9)
O(5)−H(5)···N(2B)	0.88(2)	1.74(3)	2.617(9)	170(7)
O(6)−H(6)···S(1C)	0.88(2)	2.27(3)	3.131(5)	167(6)

[a] Symmetry operations for equivalent atoms: A, $(1-x, 1-y, -z)$; B, $(3/2-x, 1-y, 1/2+z)$; C, $(1-x, -1/2+y, 1/2-z)$; D, $(3/2-x, 1-y, -1/2+z)$; E, $(1-x, 1/2+y, 1/2-z)$.

between one sulfur of the edt ligand and a methanol ligand of an adjacent cluster. The O−H···S hydrogen bonding between adjacent clusters is shown in Figure 6c. Only the axially coordinated methanol is a hydrogen bond donor in the O−H···S bonds. These O−H···S hydrogen bonds produce a one-dimensional arrangement along the crystallographic *b* axis. Details of the hydrogen bonds are given in Table 4. In **4**, four different types of hydrogen bonds are observed [O−H···S(edt), O−H···N(monodentate bpy), O−H···N(free bpy) and O−H···O(terminal)]; all methanol ligands are hydrogen-bond donors, and all uncoordinated nitrogen atoms and one thiolate sulfur of an edt ligand act as hydrogen-bond acceptors.

It is well established that 4,4′-bipy usually acts as a bridging ligand to bind two metal centers, producing coordination polymers. In contrast, 4,4′-bipy as a monodentate ligand is rare. To our knowledge, only two examples of complexes containing monodentate 4,4′-bipy ligands have been reported: the binuclear $[Cu_2L_2(4,4'\text{-bipy})_2]$ (H_2L = 1,1-(1,3-phenylene)-bis-4,4-dimethylpentane-1,3-dione)[24] and the mononuclear $[Cu(dien)(4,4'\text{-bipy})(H_2O)](ClO_4)_2$ (dien = diethylenetriamine).[25]

It has been reported previously that uncoordinated 4,4′-bipy molecules participate in the construction of supramolecular architectures through hydrogen-bond interactions with the solvent ligands bound to metal sites in polymeric frameworks.[26] Thus, in $[Zn(H_2O)_4(4,4'\text{-bipy})][NO_3]_2\cdot 4,4'\text{-bipy}$, $[Zn(H_2O)_4(4,4'\text{-bipy})][NO_3]_2\cdot 2(4,4'\text{-bipy})\cdot 3H_2O$, $[Zn(H_2O)_4(4,4'\text{-bipy})][O_3SCF_3]_2\cdot 2(4,4'\text{-bipy})$, and $[Fe(H_2O)_3(ClO_4)(4,4'\text{-bipy})][ClO_4]\cdot 1.5(4,4'\text{-bipy})\cdot H_2O$,[26b] the uncoordinated 4,4′-bipy interacts with the water ligands of the one-dimensional $[Zn-4,4'\text{-bipy}]_n$ or $[Fe-4,4'\text{-bipy}]_n$ coordination

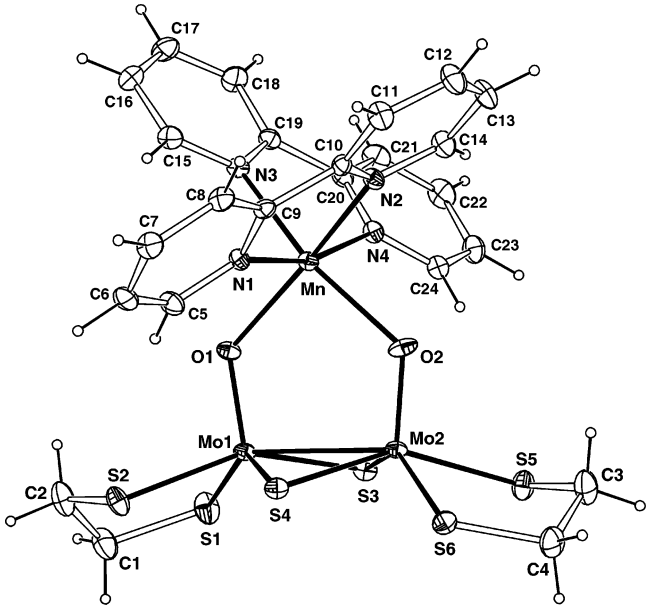

Figure 7. Molecular structure of $[Mn\{Mo_2O_2S_2(edt)_2\}(2,2'\text{-bpy})_2]$ **5** (30% displacement ellipsoids). The uncoordinated methanol molecules are not shown.

Table 5. Selected Bond Distances (Å) and Angles (deg) for $[Mn\{Mo_2O_2S_2(edt)_2\}(2,2'\text{-bpy})_2]\cdot 2MeOH$ (**5**)

Mo−S	2.3187(11)−2.436(9)	Mo(1)−Mo(2)	2.8246(5)
Mo(1)−O(1)	1.750(2)	Mo(2)−O(2)	1.747(3)
Mn−N(1)	2.237(3)	Mn−N(2)	2.240(4)
Mn−N(3)	2.256(4)	Mn−N(4)	2.238(4)
Mn−O(1)	2.235(3)	Mn−O(2)	2.246(3)
N(1)−Mn−N(2)	73.16(13)	N(3)−Mn−N(4)	74.01(13)
O(1)−Mn−O(2)	95.23(11)	N(1)−Mn−N(4)	166.25(13)
Mo(1)−O(1)−Mn	124.33(16)	Mo(2)−O(2)−Mn	124.20(17)
Mo(2)−Mo(1)−O(1)	97.86(10)	Mo(1)−Mo(2)−O(2)	98.02(11)
Mo(1)−S(3)−Mo(2)	74.31(3)	Mo(1)−S(4)−Mo(2)	74.52(3)

polymeric chains, forming hydrogen-bonded two-dimensional supramolecular networks.

Some Mn^{II}−4,4′-bipy-based polymers have been reported[27] in which 4,4′-bipy usually acts as a bridging ligand between two Mn^{II} centers. In contrast, **4** does not contain a bridging 4,4′-bipy ligand. Despite various attempts, we could not produce complexes in which 4,4′-bipy bridged two metal centers in our system. Thus, heating the reaction solution containing **4** gave no new product. It seems likely that the combination of the bulky $[Mn\{Mo_2O_2S_2(edt)_2\}]$ and the rigid 4,4′-bipy, together with the absence of any flexible and long tether group to link the two pyridine rings, means that two $[Mn\{Mo_2O_2S_2(edt)_2\}]$ fragments prevent two Mn centers being bridged by 4,4′-bipy.

Structure of 5. The molecular structure of **5** is a discrete heterometallic trinuclear cluster with an asymmetric configuration, as shown in Figure 7. Selected bond distances and angles are given in Table 5. Unlike **1**−**4**, both oxo ligands of $[Mo_2O_2S_2(edt)_2]$ are coordinated to Mn, forming an approximately planar [Mn−O−Mo−Mo−O] five-membered

(24) Clegg, J. K.; Lindoy, L. F.; McMurtrie, J. C.; Schilter, D. *J. Chem. Soc., Dalton Trans.* **2005**, 857.
(25) Julve, M.; Verdaguer, M.; Faus, J.; Tinti, F.; Moratal, J.; Monge, A.; Gutiérrez-Puebla, E. *Inorg. Chem.* **1987**, *26*, 3520.
(26) (a) Blake, A. J.; Hill, S. J.; Hubberstey, P.; Li, W.-S. *J. Chem. Soc., Dalton Trans.* **1997**, 913. (b) Carlucci, L.; Ciani, G.; Proserpio, D. M.; Sironi, A. *J. Chem. Soc., Dalton Trans.* **1997**, 1801. (c) Li, M.-X.; Xie, G.-Y.; Gu, Y.-D.; Chen, J.; Zheng, P.-J. *Polyhedron* **1995**, *14*, 1235. (d) Chen, X.-M.; Tong, M.-L.; Luo, Y.-J.; Chen, Z.-N. *Aust. J. Chem.* **1996**, *49*, 835.
(27) (a) Hou, H.-W.; Wei, Y.-L.; Fan, Y.-T.; Du, C.-X.; Zhu, Y.; Song, Y.-L.; Liu, Y.-Y.; Xin, X.-Q. *Inorg. Chim. Acta* **2001**, *319*, 212. (b) Shi, Z.; Zhang, L.-R..; Gao, S.; Yang, G.-Y.; Hua, J.; Gao, L.; Feng, S.-H. *Inorg. Chem.* **2000**, *39*, 1990.

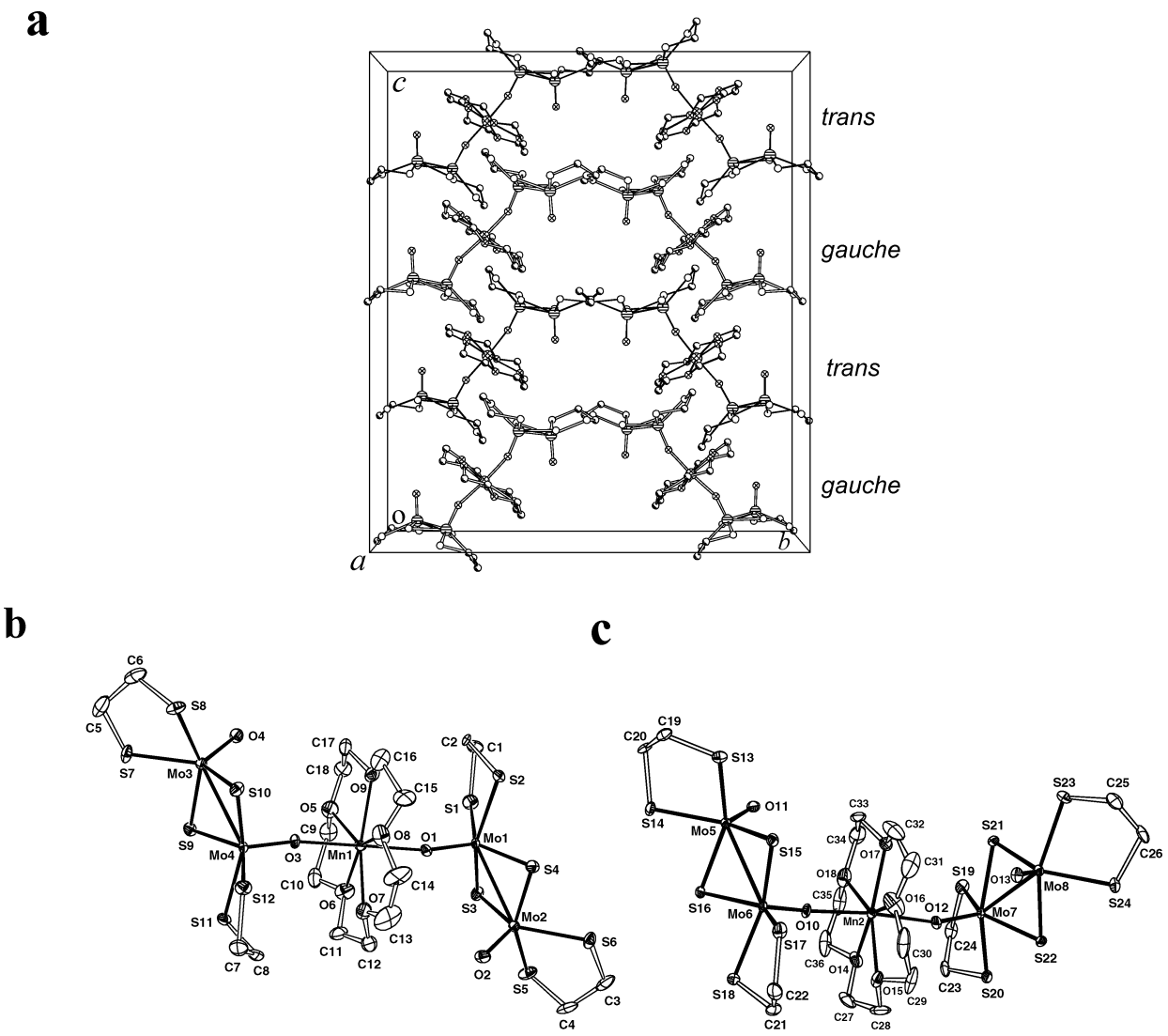

Figure 8. (a) View of the unit cell contents of **6** down the crystallographic *a* axis, showing the trans (top, first row) and gauche (top, second row) configurations of the clusters located in alternate layers. The cations and hydrogen atoms have been omitted for clarity. (b) Structure of $[Mn(15\text{-crown-}5)\{Mo_2O_2S_2(edt)_2\}_2]^{2-}$ with the trans configuration in **6** (30% displacement ellipsoids). Hydrogen atoms are omitted. (c) Structure of $[Mn(15\text{-crown-}5)\{Mo_2O_2S_2(edt)_2\}_2]^{2-}$ with the gauche configuration in **6** (30% displacement ellipsoids). Hydrogen atoms are omitted.

ring (largest deviation less than 0.06 Å from the mean plane through the five atoms). The two Mn−O bond distances are 2.235(3) and 2.246(3) Å. The metal−metal bond of Mo(1)−Mo(2), at 2.8246(5) Å, is slightly shorter than those in compounds **1**−**4** [2.8447(6)−2.8665(7) Å]. The Mn···Mo separations for Mn···Mo(1) and Mn···Mo(2) are 3.531 and 3.537 Å, respectively. These Mn···Mo separations are beyond the sum of van der Waals radii for Mn [1.70 Å] and Mo [1.70 Å], showing that there is no metal−metal bonding between Mn and Mo centers. If the $[Mo_2O_2S_2(edt)_2]$ subunit is viewed as a bidentate ligand (with oxygen donor atoms), compound **5** can be alternatively described as a complex in which the Mn^{II} is chelated by two crystallographically independent 2,2′-bpy ligands and one $[Mo_2O_2S_2(edt)_2]^{2-}$ via four nitrogen and two terminal oxo donors, forming a distorted octahedral geometry. The three chelate bite angles at Mn are N(1)−Mn−N(2) = 73.16(13)°, N(3)−Mn−N(4) = 74.01(13)°, and O(1)−Mn−O(2) = 95.23(11)°. As expected, each 2,2′-bpy ligand is essentially coplanar with Mn and the twist angle between the two pyridine rings in each 2,2′-bpy ligand is less than 4°.

Structure of 6. The solid-state structure of **6** is unusual since it contains two crystallographically independent anions with the same chemical composition. Both anions are $[Mn(15\text{-crown-}5)\{[Mo_2O_2S_2(edt)_2\}_2]^{2-}$, but they differ in the relative orientations of the two $[Mo_2O_2S_2(edt)_2]$ ligands bound to Mn (trans and gauche configurations).

A view of the unit cell contents, viewed down the crystallographic *a* axis, is illustrated in Figure 8a. There are alternating layers of stacked trans or gauche configurations of the cluster anions. The layer stacking mode can be described as an ABAB sequence along the crystallographic *c* axis. In the projection shown in Figure 8a, the two structural modes are difficult to discern. The differences can be observed in the lateral views shown in Figure 8b and c.

For the complex with the trans configuration (Figure 8b), two $[Mo_2O_2S_2(edt)_2]$ subunits are bridged by one Mn (accommodated within a 15-crown-5 macrocycle) via one

Table 6. Selected Bond Distances (Å) and Angles (deg) for $[Et_4N]_2[Mn\{Mo_2O_2S_2(edt)_2\}_2(15\text{-crown-5})]$ (**6**)

trans configuration			
Mo−S	2.2993(18)−2.4275(18)	Mo(1)−Mo(2)	2.8685(8)
Mo(3)−Mo(4)	2.8705(8)	Mo(1)−O(1)	1.724(5)
Mo(2)−O(2)	1.673(5)	Mo(3)−O(4)	1.698(5)
Mo(4)−O(3)	1.706(5)	Mn(1)−O(1)	2.119(5)
Mn(1)−O(3)	2.119(5)	Mn(1)−O(5)	2.363(6)
Mn(1)−O(6)	2.294(6)	Mn(1)−O(7)	2.176(5)
Mn(1)−O(8)	2.212(5)	Mn(1)−O(9)	2.246(5)
Mo(1)−O(1)−Mn(1)	166.4(3)	O(1)−Mn(1)−O(3)	176.3(2)
Mo(4)−O(3)−Mn(1)	168.0(3)	Mo(2)−Mo(1)−O(1)	104.78(15)
Mo(3)−Mo(4)−O(3)	105.48(16)		
gauche configuration			
Mo−S	2.3082(17)−2.4347(18)	Mo(5)−Mo(6)	2.8784(8)
Mo(7)−Mo(8)	2.8777(8)	Mo(5)−O(11)	1.693(5)
Mo(6)−O(10)	1.716(5)	Mo(7)−O(12)	1.722(5)
Mo(8)−O(13)	1.695(5)	Mn(2)−O(10)	2.133(5)
Mn(2)−O(12)	2.136(5)	Mn(2)−O(14)	2.238(5)
Mn(2)−O(15)	2.259(5)	Mn(2)−O(16)	2.197(5)
Mn(2)−O(17)	2.231(5)	Mn(2)−O(18)	2.246(5)
Mo(6)−O(10)−Mn(2)	157.5(3)	O(10)−Mn(2)−O(12)	173.6(2)
Mo(7)−O(12)−Mn(2)	155.8(3)	Mo(5)−Mo(6)−O(10)	105.62(15)
Mo(8)−Mo(7)−O(12)	105.08(16)		

terminal oxygen atom of each $[Mo_2O_2S_2(edt)_2]$ unit, forming an $MnMo_4$-based cluster anion with a nearly centrosymmetric configuration. The long Mo−O−Mn−O−Mo bridge is essentially linear [Mo(1)−O(1)−Mn(1) = 166.4(3)°, O(1)−Mn(1)−O(3) = 176.3(2)°, and Mn(1)−O(3)−Mo(4) = 168.0(3)°]. The dihedral angle between Mo(2)−Mo(1) and Mo(4)−Mo(3) is 176.6°. In the cluster with the trans configuration, the 15-crown-5 ligand is approximately planar, the largest deviation being only 0.32 Å from the mean plane based on the 15 non-hydrogen atoms of the macrocycle. The Mn accommodated within the crown ether is exactly coplanar with the mean plane of the 15-crown-5, and the five Mn−O(crown ether) bond lengths are in the range 2.176(5)−2.363(6)Å. Selected bond distances and angles are shown in Table 6.

The cluster with the gauche configuration (Figure 8c) has a similar structure to that with the trans configuration. However, in the gauche configuration the $Mo_2\cdots Mn\cdots Mo_2$ backbone is more twisted, the internal dihedral angle between Mo(5)−Mo(6) and Mo(7)−Mo(8) being 81.0°. Thus, the two forms of $[Mn(15\text{-crown-5})\{Mo_2O_2S_2(edt)_2\}_2]^{2-}$ can be viewed as rotamers.

For the cluster with the trans configuration, the molecular configuration is nearly centrosymmetric and, consequently, the centroid of this cluster anion is close to the position of the Mn atom. However, for the cluster with the gauche configuration, the centroid of the anion must be different, resulting in the gauche form being more polarizable than the trans form.

Because of the approximately planar structure of the crown ether ligand in the cluster with the gauche configuration, the direction perpendicular to the plane of the macrocycle is associated with little (if any) steric hindrance. Consequently, it seems likely that the two $[Mo_2O_2S_2(edt)_2]$ fragments in *gauche*-$[Mn(15\text{-crown-5})\{Mo_2O_2S_2(edt)_2\}_2]^{2-}$ can rotate, causing the anion to change its molecular polarizability. Furthermore, **6** crystallizes in a non-centrosymmetric, polar space group ($Pca2_1$). Thus, **6** may have potential application for nonlinear optical materials.[28] It seems likely that in solution various configurations of $[Mn(15\text{-crown-5})\{Mo_2O_2S_2(edt)_2\}_2]^{2-}$ occur, but on crystallization at room temperature only the two forms identified crystallographically are observed.

Structural Interconversions. The structural conversions of **2** into **3** and **2** into **1** have been investigated (see Experimental Section). Compounds **2** and **3** have similar compositions but are prepared under slightly different conditions. To investigate the conversions of **2** into **3** or **1**, we performed the following experiments. A pure sample of **2** was dissolved in hot methanol (ca. 50 °C). The resulting solution was allowed to crystallize, and the product was shown (by X-ray crystallography) to be **3**. Similarly, dissolution of **2** in a methanol/MeCN mixture produced crystals of **1**.

A possible mechanism for the conversion of **2** into **3** is described in Scheme 3. It is proposed that the polymeric structures of both the cationic and anionic chains in **2** are not maintained in solution, but rather form small molecular aggregates or mononuclear fragments associated with methanol ligands as fragments **A** and **D**, respectively. In this process, a nitrogen donor of each bridging TDP ligand dissociates from one Mn center, producing vacant sites on Mn which can then be occupied by methanol. At the same time, ligand substitution can occur between fragments **A** and **D**. One water ligand dissociates from the fragment **A**, and the resulting vacant site on Mn becomes occupied by an $[Mo_2O_2S_2(edt)_2]^{2-}$ unit, which has dissociated from fragment **D**. The vacant site thus created on Mn in fragment **D** can now be attacked by a water molecule, forming fragment **B**. Fragment **B** can undergo geometrical isomerization to give fragment **C**. This geometrical isomerization is possibly driven by the formation of intramolecular hydrogen bonds between the coordinated water and oxo ligands of $[Mo_2O_2S_2(edt)_2]^{2-}$, which may afford additional stability and rigidity to fragment **C**. On crystallization (polymerization step), the methanol trans to the water ligand is replaced by a TDP ligand from another fragment **C**, resulting in the polymeric **3**.

The conversion of **2** into **1** can be carried out in a methanol/MeCN mixture at room temperature. The mechanism for this conversion could be similar to that shown in Scheme 3 for the conversion of **2** into **3** but must involve more complex steps, such as the replacement of acetonitrile ligands by water, and the dissociation of the TDP molecule.

Thermogravimetric Investigations of 1 and 2. The effect of temperature on **1** and **2** has been studied using thermogravimetric analysis combined with mass spectrometry (TG-MS). The technique allows the detection of any gaseous products evolved during thermal treatment of a solid. For **1**, we are concerned with the evolution of acetonitrile and methanol ligands during heating because of the existence of coordinated and uncoordinated acetonitrile and methanol. The pertinent cleavage reactions observable in the mass

(28) Kanis, D. R.; Ratner, M. A.; Marks, T. J. *Chem. Rev.* **1994**, *94*, 195.

Scheme 3. Proposed Pathway for the Conversion of **2** into **3**

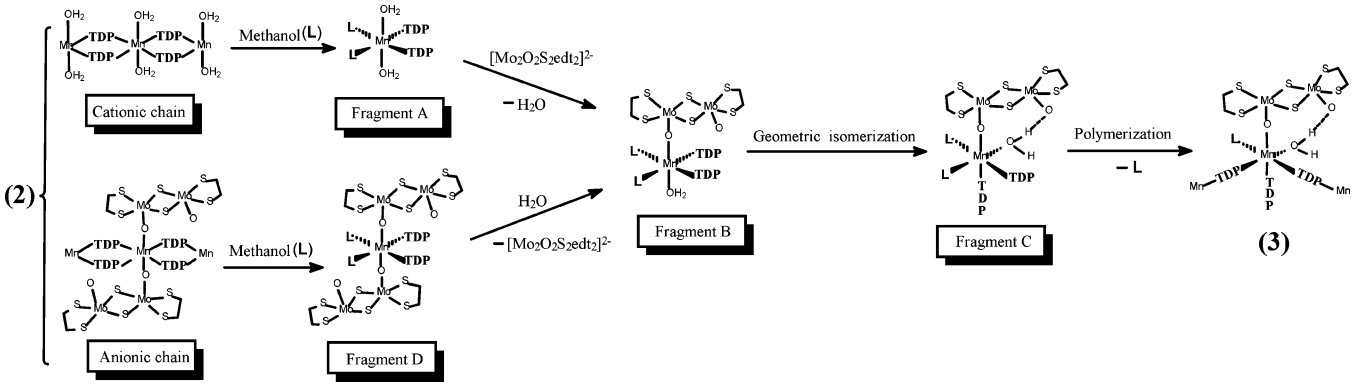

spectrometer are shown in eqs 1−3.

$$CH_3CN \rightarrow CH_3 + CN \quad (1)$$

$$CH_3OH \rightarrow CH_3 + OH \quad (2)$$

$$CH_3OH \rightarrow CH_3O + H \quad (3)$$

The principal fragments that can be detected are CH_3O ($m/e = 31$), CH_3 ($m/e = 15$), CN ($m/e = 26$), and CH_3CN ($m/e = 41$). The only source of the CH_3O fragment is methanol. The CH_3 fragment can originate from either CH_3CN or CH_3OH, whereas the CN fragment must come from CH_3CN.

On heating crystals of **1** slowly up to 500 °C, under an atmosphere of argon, a variety of products are observed, as shown in Figure 9. The TG-MS clearly shows the release of acetonitrile, which is first noticeable at ca. 180 °C. At about the same temperature CH_3O and CH_3 are also detected. The detection of CH_3O and CH_3 in the MS begin at ca. 150 °C and reaches a maximum at 200 °C. This large temperature range may be due to the release of uncoordinated and bound methanol. These observations indicate that the uncoordinated solvent molecules are held by weak forces, since the boiling point of both acetonitrile and methanol is ca. 80 °C. Presumably, the uncoordinated solvent molecules are held in the crystal structure by a number of van der Waals interactions within the polymer framework. Furthermore, as shown in Figure 2, the coordinated acetonitrile molecules are buried in the "socket" of unit **B**, perhaps resulting in bound acetonitrile being more thermally stable than the coordinated methanol in **1**. At 220 °C, a peak due to CN is observed, which is attributed to the pyrolysis of coordinated acetonitrile. The secondary CH_3 peak observed at ca. 250 °C can also be attributed to the pyrolysis reaction of acetonitrile. That coordinated acetonitrile cleaves at ca. 250 °C is consistent with the coordinated acetonitrile being thermally more stable than free acetonitrile or the coordinated methanol molecules. Whether or not the Mn center influences this cleavage reaction is unclear. The TG-MS results are consistent with the presence of two types of acetonitrile in **1** which are evident from the crystallographic investigation.

The thermogravimetic analysis curve (top of Figure 9) shows the loss of weight of **1** as the temperature is increased. The curve indicates that the first obvious weight loss is about 9% and occurs between 130 and 170 °C, corresponding to the loss of the uncoordinated solvent molecules ($1.5CH_3OH + 0.125MeCN$) and one coordinated methanol ligand (theoretical calculated weight loss = 8.95%). Subsequent weight loss occurs as a gradual process up to ca. 220 °C with about 4% additional weight loss, corresponding to the loss of the coordinated acetonitrile ligand (theoretical calculated weight loss = 4.3%). Finally, an obvious additional weight loss of ca. 17% occurs between 220 and 300 °C. This final stage involves the decomposition of polymeric framework with the complex pyrolytic-cracking of the TDP and edt ligands at high temperature. Above 300 °C, the sample continues to lose weight gradually up to 500 °C.

In the thermoanalytical investigation of **2**, we are concerned with understanding the thermal stability of edt and TDP ligands in this compound. Upon gradually increasing

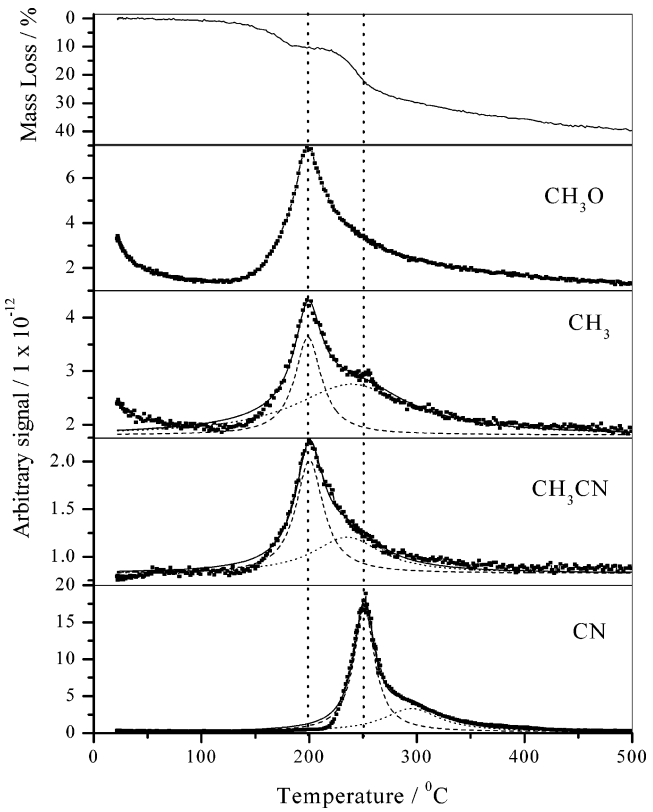

Figure 9. (top) Thermogravimetric trace obtained upon heating **1** from 20 to 500 °C under an atmosphere of argon. The traces underneath show temperature profiles of the various ions (CH_3O, CH_3, CH_3CN, and CN) detected during the thermogravimetric experiment.

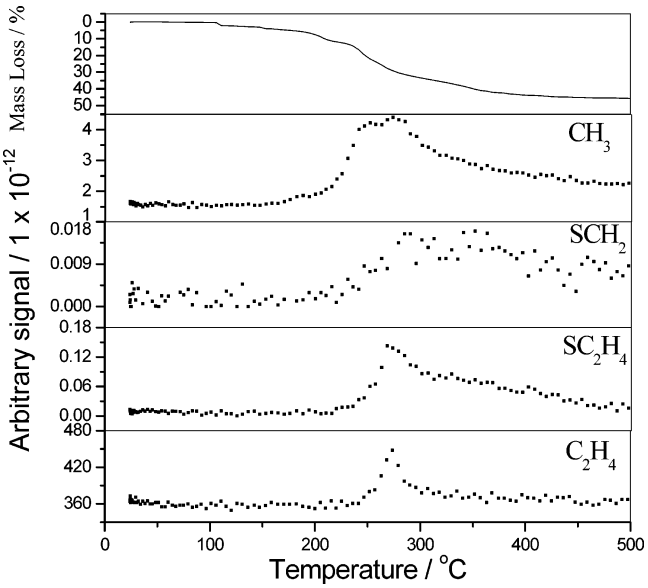

Figure 10. (top) Thermogravimetric trace obtained upon heating **2** from 20 to 500 °C under an atmosphere of argon. The traces underneath show temperature profiles of the various ions (CH_3, SCH_2, SC_2H_4, and C_2H_4) detected during the thermogravimetric experiment.

the temperature to 500 °C under an atmosphere of argon for a sample of **2**, the following species were detected in the TG-MS apparatus: CH_3 ($m/e = 15$); $[CH_2-CH_2]^{2+}$ ($m/e = 14$); SCH_2 ($m/e = 46$); and SC_2H_4 ($m/e = 60$), indicating that the edt ligands decompose above ca. 250 °C.

The thermogravimetric curve at the top of Figure 10 shows the progressive weight loss of **2**. In the temperature range 100−200 °C, there is ca. 10% weight loss, which is attributed to the release of six uncoordinated methanol molecules per molecular unit of **2** (theoretical calculated weight loss = 9.1%). However, no CH_3 fragment is observed in the mass spectrum, indicating that methanol does not undergo C−O bond cleavage in this temperature range. In the range 200−240 °C, **2** loses less than 3 wt%. A further substantial mass loss (ca. 25%) occurs in the temperature range 240−350 °C, which corresponds to the decomposition of the polymeric framework of **2** and the pyrolytic-cracking of the TDP and edt ligands. Consequently, in this high-temperature range, CH_3 and C_2H_4, as well as traces of SCH_2 and SC_2H_4, are observed. At higher temperature, the pyrolysis becomes important, as indicated by the large quantity of C_2H_4 and CH_3 observed.

Up to 250 °C, trace amounts of SCH_2 (peaks at 290 and 350 °C) and SC_2H_4 (peak at 270 °C) were observed. These fragments presumably result from pyrolysis, involving elimination reactions from the edt ligands. It is impossible to unambiguously identify the origin of the CH_3 and C_2H_4 fractions because both CH_3 and C_2H_4 can be obtained from the pyrolysis of both TDP and edt ligands.

Magnetic Properties of 1−6. The magnetic susceptibilities of compounds **1**−**6** have been investigated at room temperature. The corresponding magnetic moments μ_{eff} for **1**−**6** are as follows. **1**, 5.83; **2**, 8.98; **3**, 5.86; **4**, 5.85; **5**, 5.91; and **6**, 3.90 μ_B. If the orbital contribution to the magnetic moment from molybdenum atoms is ignored, these μ_{eff} values indicate that compounds **1**, **3**, **4**, and **5** contain five unpaired electrons, while **2** and **6** have eight and three unpaired electrons, respectively. In all the compounds **1**−**6**, the Mo−Mo bond distances fall in the short range 2.8−2.9 Å, consistent with strong coupling of two $4d^1$ electrons from each of the Mo^V centers. The $[Mo^V_2O_2S_2(edt)_2]^{2-}$ subunit is thus diamagnetic, as are other complexes containing the Mo^V_2 core.[29] Furthermore, the closest Mn···Mn separations in compounds **1**−**6** are ca. 7.6, 10.5, 10.1, 8.1, 8.3, and 10.4 Å, respectively. All these Mn···Mn distances are significantly longer than the distance associated with metal−metal contact (3.4 Å). Furthermore, the TDP molecule has a nonconjugative $-(CH_2)_3-$ spacer between the two pyridyl groups, and hence magnetic coupling or magnetic exchange[30] between Mn···Mn must be very weak or nonexistent in **1**−**6** at room temperature.

All the compounds **1**, **3**, **4**, and **5** contain the $[Mn\{Mo_2O_2S_2(edt)_2\}]$ fragment, and they all display similar magnetic properties at room temperature, with the experimental μ_{eff} values being close to the spin-only theoretical μ_{eff} value 5.92 μ_B. This observation suggests that Mn^{II} in **1**, **3**, **4**, and **5** is in a high-spin state with $S = 5/2$; it seems likely that, for all four compounds, the observed magnetic moment is dominated by the Mn^{II} atom.

Compounds **2** and **6** exhibit unusual magnetic moments at room temperature, with much lower μ_{eff} values than the spin-only theoretical value. If it is assumed that Mn^{II} in **2** and **6** is in a high-spin state and there is no magnetic superexchange of Mn(3d)···Mo(4d), the corresponding theoretical μ_{eff} values should be 10.95 μ_B for **2** and 5.92 μ_B for **6**, corresponding to 10 and 5 unpaired electrons, respectively. It is worth noting that both **2** and **6** contain the $[Mn\{Mo_2O_2S_2(edt)_2\}_2]^{2-}$ fragment and it appears that this fragment exhibits lower μ_{eff} values than predicted using the spin-only formula. It seems likely that there is significant magnetic coupling at room temperature.

Summary

The synthesis of assemblies formed by attaching Mn^{II} to $[Mo_2O_2S_2(edt)_2]^{2-}$ by means of the oxo ligands has been described in this paper, and the nature of the resulting complex has been shown to depend on the reaction conditions and the solvent. The reactions occur under mild conditions. The binding of the solvent to the complex is a key factor in determining the structure of the compound that crystallizes from solution.

In the reaction solution containing Mn^{II}, $[Mo_2O_2S_2(edt)_2]^{2-}$ and TDP or 4,4′-bipy, acetonitrile and methanol serve as both the reaction solvent and the ligands to the Mn. The existence of competition between multidentate ligands and solvent molecules binding to Mn is general in polymerization processes.

(29) (a) Coucouvanis, D. *Adv. Inorg. Chem.* **1998**, *45*, 1. (b) We have determined the magnetic moment of $[NEt_4]_2[Mo_2O_2S_2(edt)_2]$ at room temperature, $\mu_{eff} = 0$.

(30) (a) Barandika, M. G.; Hernández-Pino, M. L.; Urtiaga, M. K.; Cortés, R.; Lezama, L.; Arriortua, M. I.; Rojo, T. *J. Chem. Soc., Dalton Trans.* **2000**, 1469. (b) Rodríguez-Martín, Y.; Hernández-Molina, M.; Sanchiz, J.; Ruiz-Pérez, C.; Lloret, F.; Julve, M. *J. Chem. Soc., Dalton Trans.* **2003**, 2359.

There are significant differences in the structural features of complexes **1**−**3** related to the use of distinct solvents or reaction temperature. Thus, **1** contains acetonitrile and methanol molecules bound to Mn, whereas **2** has a cationic chain in which two water molecules bind to the Mn and an anionic chain in which no solvent molecule is incorporated. **3** contains both water and methanol coordinated in cis positions to Mn, which leads to the pyridyl ligands from the three TDP ligands bound to Mn in a *fac* disposition. Thus, among the factors involved in the synthesis of compounds **1**−**3**, the solvent clearly influences the structure of the resulting framework. In addition, **4** has four molecules of methanol bound to Mn, suggesting the favorable formation of discrete clusters if the long and flexible multidentate ligands are absent in the reaction system containing Mn^{II} and $[Mo_2O_2S_2(edt)_2]^{2-}$.

Metal−sulfur clusters are often decomposed under acid conditions and high temperature. Ligating metal−sulfur clusters on the backbone of coordination polymers may modify their properties and improve their stability toward acid or high temperature. The research reported in this paper describes how to utilize the terminal oxo ligand on an Mo site to assemble molybdenum−sulfur clusters on a coordination polymer framework under mild conditions. The approach we have employed is sufficiently general that the synthesis of other new extended arrays of Mo−S−O-based clusters in combination with other metal ions can be anticipated using the same method.

Experimental Section

General. The preparations of **1**−**6** were performed in air. $[Et_4N]_2[Mo_2O_2S_2(edt)_2]$ was prepared according to the literature method.[14b] All other chemicals and reagents were used as received from commercial sources. The C, H, N microanalyses were carried out on a Carlo Erba 1108 elemental analyzer by the University of Newcastle upon Tyne microanalytical service. Infrared spectra (KBr disks) were recorded on a Perkin-Elmer 598 spectrometer.

Thermogravimetric Analysis. Thermogravimetric analysis combined with mass spectrometry (TGA-MS) for studying compounds **1** and **2** was performed with the heating rate set at 15 °C min^{-1}. Typically, ca. 6.5 mg of the crystals were used in the analysis. All experiments were conducted under an argon gas flow with a flow rate of 50 mL min^{-1}. The TG-MS apparatus consisted of a Thermal Sciences model STA 1500 thermogravimetric analyzer connected via a 1 mm internal diameter sampling probe lined with 0.32 mm internal diameter fused silica capillary to a VG Quadrupoles 300 amu quadrupole mass spectrometer. The TGA sample crucible was situated directly below the sample probe. The detection of the fragments is slightly delayed after release from the solid samples due to the long pipe used to interface the TG apparatus with the mass spectrometer. The delay time is about 2 min, which leads to the corresponding temperature for detection of the fragments being about 30 °C less than the corresponding mass loss temperature.

X-ray Crystallography Analyses. The data for **1**, **2**, **5**, and **6** were collected on a Nonius KappaCCD diffractometer by the $\phi + \omega$-scan method, while the data for **3** and **4** were collected on a Bruker SMART CCD diffractometer by the ω-scan method. All six compounds were analyzed using Mo Kα radiation ($\lambda = 0.71073$ Å) at a temperature of 150 K. Crystal data and other experimental information are given in Table 7, with further details in the Supporting Information. Semiempirical absorption corrections were applied in all cases on the basis of repeated and symmetry-equivalent reflections.[31] The structures were solved by direct methods and refined by full-matrix least-squares on all unique F^2 values.[32] Anisotropic displacement parameters were assigned to all non-hydrogen atoms. The hydrogen atoms of coordinated water (for **2** and **3**) and the hydroxyl group of coordinated methanol molecules (except for **3**) were located in difference maps and refined with appropriate geometrical restraints. Other hydrogen atoms were placed in idealized positions and allowed to ride on their respective parent atoms. Disorder for one TDP ligand in **2** and **3** was modeled in a 1:1 ratio. Disorder for the ethyl group of one edt ligand in **3**, **5**, and **6** was resolved and successfully modeled in a 3:1, 2:1, and 1:1 ratio, respectively. The uncoordinated methanol of **3** was disordered in a 1:1 ratio. In addition, for **1**, **2**, and **5**, poorly resolved methanol solvent molecules were treated by the SQUEEZE procedure in PLATON,[33] with one-and-a-half methanol molecules per asymmetric unit of **1**, three methanol molecules per asymmetric unit of **2** and two methanol molecules for each asymmetric unit of **5**. The crystal of **6** was found to be inversion-twinned.

Synthesis of 1. TDP (0.4 g, 2.0 mmol) and $Mn(NO_3)_2 \cdot 6H_2O$ (0.287 g, 1.0 mmol) were added to 60 mL of a mixed solvent (methanol/acetonitrile = 2:1), then stirred at room temperature in air for 30 min. $[Et_4N]_2[Mo_2O_2S_2edt_2]$ (0.732 g, 1.0 mmol) was then added, and the reaction mixture stirred continuously for 30 min. The resulting orange solution was allowed to evaporate slowly under ambient conditions. After 3 h, a small amount of orange cuboidal crystals was isolated from solution. Continuous evaporation of the solution for 2 days yielded orange cuboidal crystals (0.62 g, yield 64.2% based on Mn) suitable for X-ray crystallographic analysis. **1** is slightly soluble in a methanol/acetonitrile mixed solvent but insoluble in acetonitrile. Anal. Calcd (found): C, 35.68 (35.57); H, 4.49 (4.42); N, 6.08 (6.03)%. IR (KBr pellet, cm^{-1}): υ(C≡N of acetonitrile), 2267(m); υ(pyridyl group of TDP), 1610(s), 1422(m), 1384(m); υ(Mo−O), 918(s), 889(s); υ(Mo−μ-S), 434(m).

Synthesis of 2. 2 was synthesized by a method similar to that of **1**, but using only methanol as the solvent. Evaporation of the filtrate in air for 5 days gave orange prismatic crystals (0.63 g, yield 59.7% based on Mn) suitable for X-ray crystallographic analysis. **2** is slightly soluble in methanol and fairly soluble in hot methanol. Anal. Calcd (found): C, 37.54 (37.50); H, 4.96 (4.92); N, 5.31 (5.38)%. IR (KBr peller, cm^{-1}): υ(pyridyl group of TDP), 1609(s), 1424(m), 1385(m); υ(Mo−O), 918(s), 895(s); υ(Mo−μ-S), 439(m).

Synthesis of 3. 3 was synthesized by a method similar to that of **2**, but the reaction was carried out in hot methanol (50 °C) for half an hour, then cooled to room temperature. A small amount of yellow precipitate was removed by filtration. Slow evaporation of the filtrate in air for 5 days yielded yellow octahedral crystals of **3** (0.61 g, yield 61% based on Mn) suitable for X-ray crystallographic single-crystal analysis. Anal. Calcd (found): C, 38.21 (38.19); H, 4.61 (4.58); N, 5.57 (5.58)%. IR (KBr pellet, cm^{-1}): υ(pyridyl group of TDP), 1611(s), 1422(m), 1384(m); υ(Mo−O), 919(s), 894(s); υ(Mo−μ-S), 426(m).

Synthesis of 4. 4 was synthesized by a method similar to that of **1**, using 60 mL of mixed solvent (methanol/acetonitrile = 2:1), and 4,4′-bipy (0.312 g, 2 mmol) instead of TDP. Slow evaporation of the filtrate in air for 1 week gave orange platelike crystals (0.38

(31) Sheldrick, G. M. *SADABS: Siemens Area Detector Absorption Correction Software*; University of Göttingen: Göttingen, Germany, 1996.
(32) Sheldrick, G. M. *SHELXTL*; Bruker AXS Inc.: Madison, WI, 2001.
(33) Spek, A. L. *J. Appl. Crystallogr.* **2003**, *36*, 7.

Table 7. Crystal Data and Structure Refinement Parameters for Compounds **1**−**6**[a]

	1	**2**	**3**	**4**
formula	$C_{56.5}H_{84.75}Mn_2Mo_4N_{8.25}O_9S_{12}$	$C_{66}H_{104}Mn_2Mo_4N_8O_{14}S_{12}$	$C_{32}H_{46}MnMo_2N_4O_5S_6$	$C_{23}H_{36}MnMo_2N_3O_6S_6$
fw	1901.94	2111.93	1005.91	889.73
cryst syst	tetragonal	triclinic	monoclinic	orthorhombic
space group	*P*4/*n*	$P\bar{1}$	$P2_1/n$	*Pbca*
a (Å)	27.560(5)	11.9446(11)	12.1321(5)	15.3815(8)
b (Å)	27.560(5)	12.1041(9)	19.3126(7)	18.2475(9)
c (Å)	10.5496(10)	17.3420(18)	17.2368(6)	23.9239(12)
α (deg)		89.331(9)		
β (deg)		84.978(11)	96.308(1)	
γ (deg)		63.933(8)		
V (Å^3)	8013(2)	2242.6(4)	4014.2(3)	6714.8(6)
Z	4	1	4	8
reflns measd	70 622	45 379	28 966	46 211
unique data, R_{int}	7067, 0.0890	10 260, 0.0630	7057, 0.0360	5918, 0.0797
params	390	475	593	390
R (F, $F^2 > 2\sigma$)[b]	0.0448	0.0403	0.0447	0.0512
R_w (F^2, all data)[c]	0.1147	0.1212	0.0973	0.1434
GOF on F^2	1.064	1.078	1.322	1.162
max, min electron density (e Å^{-3})	0.94, −0.48	1.42, −0.89	0.62, −0.71	1.67, −1.01

	5	**6**
formula	$C_{26}H_{32}MnMo_2N_4O_4S_6$	$C_{34}H_{76}MnMo_4N_2O_9S_{12}$
fw	903.74	1480.39
cryst syst	monoclinic	orthorhombic
space group	$P2_1/c$	$Pca2_1$
a (Å)	16.2683(10)	14.3218(15)
b (Å)	11.8808(12)	26.6005(15)
c (Å)	18.5510(7)	30.184(3)
α (deg)		
β (deg)	102.890(4)	
γ (deg)		
V (Å^3)	3495.2(4)	11499.3(18)
Z	4	8
reflns measd	48 225	71 784
unique data, R_{int}	6114, 0.0528	19 937, 0.0411
params	380	1137
R (F, $F^2 > 2\sigma$)[b]	0.0364	0.0364
R_w (F^2, all data)[c]	0.0923	0.0836
GOF on F^2	1.047	1.065
max, min electron density (e Å^{-3})	0.87, −2.72	1.30, −0.65

[a] Collected using Mo Kα ($\lambda = 0.71073$ Å) radiation at $T = 150$ K. [b] $R = \sum||F_o| - |F_c||/\sum|F_o|$. [c] $R_w = \{\sum[w(F_o^2 - F_c^2)^2]/\sum[w(F_o^2)^2]\}^{1/2}$.

g, yield 42.7% based on Mn) suitable for X-ray crystallographic analysis. Anal. Calcd (found): C, 31.05 (31.08); H, 4.08 (4.11); N, 4.72 (4.76)%. IR (KBr pellet, cm^{-1}): *ν*(pyridyl group of 4,4′-bpy), 1603(s), 1411(m), 1274(m); *ν*(Mo−O), 913(s); *ν*(Mo−*μ*-S), 449(m).

Synthesis of 5. 5 was synthesized by a method similar to that of **1** using 60 mL of mixed solvent (methanol/acetonitrile = 2:1), except that 2,2′-bipy (0.312 g, 2 mmol) was used instead of TDP. In addition, after adding $[Et_4N]_2[Mo_2O_2S_2(edt)_2]$, the mixture was stirred for only 1 min and then filtered, due to the rapid crystallization of the product. Evaporation of the filtrate in air for 1 day gave red block crystals (0.65 g, yield 72% based on Mn) suitable for X-ray crystallographic analysis. **5** is slightly soluble in methanol but insoluble in acetonitrile. Anal. Calcd (found): C, 34.55 (34.51); H, 3.57 (3.55); N, 6.20 (6.23)%. IR (KBr pellet, cm^{-1}): *ν*(pyridyl group of 2,2′-bpy), 1595(s), 1437(m); *ν*(Mo−*μ*-O), 870(s); *ν*(Mo−*μ*-S), 455(m).

Synthesis of 6. 15-crown-5 (0.20 mL, 1.0 mmol) and $Mn(NO_3)_2 \cdot 6H_2O$ (0.287 g, 1.0 mmol) were added to 30 mL of a mixed solvent (methanol/acetonitrile = 2:1) then stirred at room temperature in air for 30 min. $[Et_4N]_2[Mo_2O_2S_2(edt)_2]$ (0.732 g, 1.0 mmol) was then added, and the reaction mixture stirred continuously for 30 min. Slow evaporation of the orange solution under ambient conditions for 10 days gave orange block crystals (0.43 g, yield 58.1% based on Mo) suitable for X-ray crystallographic analysis. **6** is slightly soluble in methanol but quite soluble in acetonitrile. Anal. Calcd (found): C, 27.59 (27.58); H, 5.17 (5.15); N, 1.89 (1.88)%. IR (KBr pellet, cm^{-1}): 1744(w), 1484(s), 1271(m); *ν*(Mo−O), 933(s), 894(s); *ν*(Mo−*μ*-S), 432(m).

Investigations of Interconversions of 2 into 3 and 2 into 1. Conversion of 2 into 3. Crystals of **2** (100 mg) were dissolved in 30 mL of hot methanol and stirred for 1 h at 50 °C. All crystals of **2** were soluble, and the orange solution was cooled to room temperature and evaporated in air for 8 days. Yellow octahedral crystals (76 mg) were isolated. The crystals produced were selected for characterization by single-crystal X-ray diffraction and elemental analysis. The unit cell was monoclinic, space group $P2_1/n$, a = 12.132 Å, b = 19.313 Å, c = 17.237 Å, β = 96.308°, V = 4014 Å^3. Elemental analysis of the crystals, found: C, 38.20; H, 4.57; N, 5.56%. These results confirm that the product of this conversion reaction was identical to **3**.

Conversion of 2 into 1. Crystals of **2** (100 mg) were dissolved in 45 mL of mixed solvent (methanol/acetonitrile = 2:1) and stirred for 1 h at room temperature. Most of the crystals of **2** gradually dissolved, and the orange filtrate was evaporated in air for 5 days. Orange cuboidal crystals (58 mg) were isolated. The unit cell was tetragonal, space group *P*4/*n*, a = 27.56 Å, c = 10.550 Å, V = 8013 Å^3. Elemental analysis, found: C, 35.60; H, 4.45; N, 6.05%.

These results confirm that the product of this conversion reaction was identical to **1**.

Acknowledgment. We acknowledge the EPSRC (U.K.) for equipment funding. P.L. acknowledges a studentship from the University of Newcastle.

Supporting Information Available: X-ray crystallographic files for compounds **1**−**6**; figures showing alternative views of the double sheet networks of **1** and representations of **2**. This material is available free of charge via the Internet at http://pubs.acs.org.

IC060205U